

Distribution of Interstellar Hydrogen Atoms in the Heliosphere and Backscattered Solar Lyman- α

VLADISLAV V. IZMODENOV*

*Lomonosov Moscow State University, School of Mechanics and Mathematics,
Institute for Problems in Mechanics, Russian Academy of Sciences,
Moscow, Russia
Space Research Institute, Russian Academy of Sciences, Moscow, Russia*

OLGA A. KATUSHKINA

*Space Research Institute (IKI) Russian Academy of Sciences,
Moscow, Russia
Lomonosov Moscow State University, School of Mechanics and Mathematics,
Moscow, Russia*

ERIC QUÉMERAIS

*LATMOS-IPSL,
Université Versailles-Saint Quentin, Guyancourt, France*

MACIEJ BZOWSKI

*Space Research Center,
Polish Academy of Science, Warsaw, Poland*

Abstract

We review the modern concepts of penetration of interstellar atoms of hydrogen into the heliosphere up to 1 AU. Before entering into the heliosphere the atoms penetrate through the region of the solar wind (SW) interaction with the local interstellar medium (LISM). In the interaction region the atoms can exchange charge with both solar wind and interstellar protons disturbed in the SW/LISM interaction region. Charge exchange results in a disturbance of the pristine interstellar atom flow in the interaction region, and, therefore, the parameters of interstellar gas inside the heliosphere are different from their interstellar values. This makes it more difficult to determine local interstellar parameters from measurements of

the interstellar atoms inside the heliosphere, but, on the other side, opens possibilities to study the SW/LISM interaction region remotely. This paper overviews the main physical phenomena and modern models of the SW/LISM interaction and presents a state-of-art 3D kinetic model of the interstellar hydrogen gas inside the heliosphere. The distributions of the gas parameters are compared with the distributions obtained in the context of the classical hot model. Quantitative and qualitative differences are discussed. The state-of-art model is employed to calculate spectra of the backscattered Lyman- α radiation as they would be measured at 1 AU and the zero, first and second moments of the spectra. It is shown that the SW/LISM interaction imprints in the spatial and velocity distribution of the interstellar atoms are revealed in the intensities, line-shifts, and line-widths of the distribution functions. A qualitative comparison of the model results with SOHO/SWAN data are presented.

Introduction: A Brief Historical Review

The first evidence of the presence of interstellar atomic hydrogen in the interplanetary medium was obtained from rocket measurements of stellar ultraviolet (UV) radiation, when a strong diffuse UV radiation at 105–122.5 nm was observed instead of the expected stellar point sources. In the discussion of their rocket night-flight results, [Kupperian et al. \(1959\)](#) interpreted this emission as due to solar Lyman- α photons scattered by interplanetary H atoms. Similarly, [Shklovsky \(1959\)](#) interpreted these rocket results, together with night time H alpha measurements, in the same way. However, he mentioned an alternate explanation “.which cannot be excluded for the time being,” in which this night time Lyman- α emission would be produced by resonant scattering of H atoms linked to the Earth, in an extended atmosphere that he called the “geocorona.” In order to discriminate the sources, [Morton and Purcell \(1962\)](#) performed a night time rocket measurement of diffuse Lyman- α radiation using an absorption cell technique (for a description of the technique see, e.g., [Bertaux and Lallement 1984](#)). These measurements showed that only 15 % of the observed scattered Lyman- α radiation was at a wavelength shifted by more than 0.004 nm from the line center. 85 % of the absorbed radiation was produced by transport of Lyman- α photons from the day side to the night side by radiative transfer in an extended exosphere, while the remaining 15 % was highly Doppler-shifted, possibly produced by precipitating magnetospheric protons, or of extra-terrestrial origin. To produce such wavelength-shifted photons, the scattering gas should be either hot (to produce a broad spectral linewidth) or in motion with respect to the Sun (to produce Doppler-shifted protons).

[Patterson et al. \(1963\)](#) proposed a scenario for the hot atomic hydrogen within the heliosphere and obtained the first analytical expression for the distribution of the atomic hydrogen in interplanetary space. This work was based on the concept of the heliospheric interaction with the surrounding interstellar (or galactic) medium suggested by [Axford et al. \(1963\)](#) and shown schematically in Fig. 2.1.

It was assumed in the model that the solar wind blows continuously and is spherically symmetric outward from the Sun with a nearly constant, highly supersonic

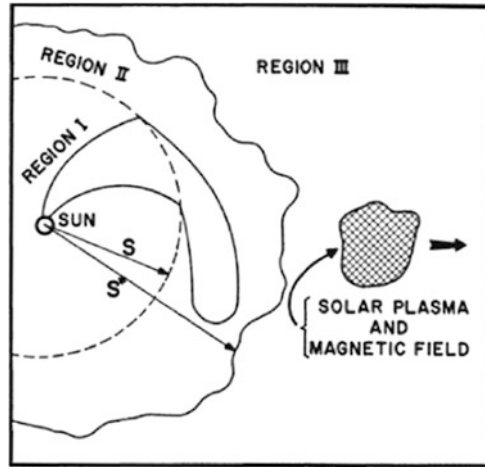


Figure 2.1: A sketch of the structure of the interaction region between the solar wind and the interstellar magnetic field proposed by [Axford et al. \(1963\)](#). The solar wind is supersonic in Region I, and the solar magnetic field lines form Archimedean spirals co-rotating with the Sun. The termination shock is located at a heliospheric distance S . Beyond the termination shock, in region II (the boundary shell), solar-wind protons and interstellar neutral hydrogen atoms exchange charge, and dissipative effects permit oppositely-directed solar wind magnetic-field lines to merge and form closed loops. S^* is the distance to the boundary between the solar and interstellar magnetic fields. Blobs of the solar plasma and magnetic field detach from region II and move out into region III (interstellar space), where they gradually diffuse away

velocity. Hence, the solar wind density and dynamic pressure are directed radially away from the Sun and decrease as $\sim 1/r^2$. At the distance where the dynamic pressure (magnetic pressure and/or thermal pressure) equals the pressure of the local interstellar medium (LISM), the solar wind passes through a standing shock—the termination shock (TS), beyond which it slows down and becomes subsonic. Nevertheless, it was assumed that in the region beyond the shock front (that we call now the inner heliosheath), the individual velocities of solar wind protons remain of the order of ~ 300 km/s due to high thermal velocities. The energetic protons undergo charge exchange with neutral interstellar hydrogen. This process leaves low-energy protons in the transition region beyond the shock, and provides an *isotropic* source of high-energy neutral hydrogen atoms. Some of these atoms (now called energetic neutral atoms—ENAs) move through the termination shock (TS) back toward the Sun.

[Patterson et al. \(1963\)](#) calculated the distribution of the neutral hydrogen atoms in interplanetary space assuming that the TS is an isotropic source of the neutrals, taking into account their velocity, the ionizing solar radiation, and the charge exchange with the solar wind. It was also assumed that (1) the post-shocked solar

wind protons suffer charge exchange with interstellar neutrals just in a thin shell beyond the TS, (2) half of the solar wind flux is returned into the heliosphere in the form of fast neutrals. Later, [Hundhausen \(1968\)](#) showed that most of the neutral hydrogen observable in the vicinity of the Earth does not undergo charge exchange between solar wind protons and interstellar neutral hydrogen near the shock boundary of the heliosphere, as assumed by [Patterson et al. \(1963\)](#), but in a region far beyond the shock. Hundhausen's model predicted much smaller atomic hydrogen density near Earth. Therefore, the neutral hydrogen density near Earth could then only be maintained in the model if the shock is near 5 AU.

An alternative approach, that actually became a commonly accepted paradigm for at least two decades, was suggested by [Fahr \(1968a\)](#). We should point out that modern concepts of the ENAs originating in the inner heliosheath ([Gruntman et al. 2001](#)) are very similar to those of [Patterson et al. \(1963\)](#) and [Hundhausen \(1968\)](#).

[Fahr \(1968a\)](#) pointed out that the assumption of the random motion of interstellar hydrogen made by [Patterson et al. \(1963\)](#) is very unlikely because the solar system itself has a velocity of 20 km/s with respect to the local standard of rest of nearby stars, and also interstellar hydrogen clouds are moving. It was shown ([Blum and Fahr 1970](#); [Axford 1972](#)) that the concept of the Strömgren sphere of ionized gas around a hot star fails for the Sun, in case that there is a relative bulk motion of the interstellar atoms with respect to the Sun. The Strömgren sphere is determined by equating the flux of ionizing photons emitted by the Sun to the total recombination rate ([Strömgren 1939](#)). In case of the Sun, the Strömgren sphere has a radius of about 1,500 AU. It was estimated ([Blum and Fahr 1970](#)) that about 90 % of the cold interstellar hydrogen with a velocity of 20 km/s will enter the heliosphere without being photoionized or charge exchanged.

[Fahr \(1968a\)](#) has calculated the heliospheric distribution of the number density of the cold interstellar hydrogen taking into consideration the macroscopic motion of interstellar gas and the solar gravitational field. [Blum and Fahr \(1970\)](#) took into account the losses of interstellar atoms due to charge exchange with the solar wind protons and due to photoionization by solar radiation. Therefore, in the model, the cold interstellar neutrals enter the solar system along Kepler trajectories and suffer losses caused by the EUV-ionization and charge exchange with the solar wind protons. The charge exchange process produces secondary fast neutrals having the velocity of the solar wind. These particles move radially outwards without significant losses within the solar wind ([Fahr 1968b](#)), and cannot be observed in Lyman- α because they are Doppler shifted too far from the center of the solar line.

According to the prediction of the cold model of [Blum and Fahr \(1970\)](#), the number density of interstellar H atoms are larger in the direction toward the interstellar flow, and, therefore, the observed Lyman- α emission should have a maximum, and the maximum should be toward the direction of the interstellar H atom flow. Extraterrestrial UV radiation (most likely Lyman- α) was measured from interplanetary probes Zond 1 ([Kurt 1966, 1967](#)), of Venera 2, 3, and 4 ([Kurt and Germogenova 1967](#); [Kurt and Syunyaev 1968](#)), and of Mariner 5 and 6 ([Barth 1970](#)). These measurements proved that the 15 % highly shifted night time Lyman- α found earlier by [Morton and Purcell \(1962\)](#) in their rocket flight was indeed of extra-terrestrial origin. It was found in these interplanetary probes measurements that the backscattered Lyman- α emission is distributed inhomogeneously

and features toward the direction of the galactic center. Because of this specific direction of the emission maximum, a new “galactic” source of the diffuse radiation was suggested as an alternative to [Patterson et al. \(1963\)](#) scenario.

The dilemma of the galactic or interstellar origin of the diffuse radiation was resolved by OGO-5 spacecraft measurements ([Bertaux and Blamont 1971](#); [Thomas and Krassa 1971](#); [Lallement 2001](#)). The apogee of OGO-5 was out of the geocorona, i.e. the geocorona emission could be ruled out at apogee. The spacecraft was spinning so that the extraterrestrial diffuse Lyman- α radiation could be mapped over the sky. A broad maximum in one direction and a minimum in the opposite direction were observed. To find the distance to the region of the maximum emissivity of the backscattered Lyman- α emission two sky-mappings of the diffuse Lyman- α were performed on board the OGO-5 spacecraft in September 1970 and April 1970, when the Earth (and the spacecraft too) was at opposite positions in its orbit. The difference in the position of the maximum of diffuse Lyman- α emission as seen in the two maps was by about 30° . This proved that the emission region was located at few AU from the Sun and the displacement of the maximum was due to the parallax effect that would be negligibly small in the case of a galactic source of the emission. Analysis of three sky-maps of the OGO-5 allowed to find the direction of the interstellar H atoms approaching the Sun ([Bertaux et al. 1972](#)). Newer values of the direction of interstellar hydrogen inside the heliosphere are (252.5° , 8.9°) in the ecliptic J2000 coordinates ([Lallement et al. 2010](#)).

Therefore, the theoretical prediction made by [Fahr \(1968a\)](#) and [Blum and Fahr \(1970\)](#), i.e. that interstellar H atoms penetrate into the heliosphere up to distances of a few AU from the Sun, was confirmed by Lyman- α measurements made by OGO-5 spacecraft instruments in 1969–1970 ([Bertaux and Blamont 1971](#); [Thomas and Krassa 1971](#); [Thomas 1972](#)), and the “galactic” interpretation was ruled out. An upper limit of galactic emission of 15 Rayleigh (compared to the observed 300–500 R of the extra-terrestrial emission) was derived from hydrogen absorption cell measurements on board Prognoz-5 and 6 ([Lallement et al. 1984](#)).

Since the interstellar temperature is $\sim 10^4$ K, the real situation is drastically different from the cold model considered above. The cold model fails for the downwind direction at the axis of symmetry, where it gives infinite densities in case when the solar gravitation is larger than the radiation pressure ($\mu < 1$). The quantity μ is defined as the ratio of the solar gravitational attraction to the repulsion due to radiation pressure and will be used throughout this document:

$$\mu = |\mathbf{F}_{rad}|/|\mathbf{F}_g|. \quad (2.1)$$

Actually, [Danby and Camm \(1957\)](#) were the first to solve the problem of the motion of a cloud of gas particles in the gravitational field of a point mass. They found an analytical formula for the velocity distribution function of the particles. Later, the Danby–Camm formula was applied to the interstellar atoms moving in the heliosphere and modified by including a loss function to take into account the effects of charge exchange and photoionization. Details of the hot model formulation will be given later in this paper ([Lallement et al. 1985a](#); [Izmodenov 2006](#)).

The problem with finite temperature has been considered by Fahr (1971), Thomas (1972), Feldman et al. (1972), Bertaux et al. (1972), Fahr (1974), Blum et al. (1975), Meier (1977), Fahr (1978), and Wu and Judge (1979). Such a model is called the classical hot model of hydrogen distribution. Very recently this classical hot model has been applied by Lee et al. (2012) to analyses of atom fluxes measured at 1 AU by the Interstellar Boundary Explorer (IBEX). Measurements of the backscattered solar Lyman- α radiation with a hydrogen absorption cell on board the Soviet interplanetary probe Mars-7 (Bertaux et al. 1976) brought information on the spectral profile of the extraterrestrial Lyman- α radiation. More accurate measurements with a hydrogen absorption cell flown on Prognosz-5, interpreted with the assumption of a Gaussian velocity distribution of H atoms, yielded a temperature of $(8.8 \pm 1) \cdot 10^3$ K (Bertaux et al. 1977). However, a more accurate interpretation of the spectral profile is only possible if the velocity distribution function of the interstellar hydrogen is taken into account, even for the simple case of $\mu = 1$, in which atoms trajectories are straight lines.

In the 1980–1990s the classical hot model was widely used to interpret backscattered solar Lyman- α measurements. However, very soon it became clear that effects connected with the heliolatitudinal and solar cycle variations of the solar wind must be taken into account.

It has been shown through modeling by Joselyn and Holzer (1975) that a non-isotropic solar wind would strongly affect the distribution of atomic hydrogen in the heliosphere, and that this could be observed in maps of backscattered solar Lyman- α radiation. The signatures of the latitudinal variations were observed in the backscattered interplanetary Lyman- α glow observations from Mariner 10 (Kumar and Broadfoot 1978, 1979; Witt et al. 1979, 1981), Prognosz 6 (Lallement et al. 1985b; Summanen et al. 1993), Pioneer–Venus (Ajello et al. 1987; Lallement and Stewart 1990), SOHO/SWAN (Bertaux et al. 1997, 1999), and by the Ulysses GAS Lyman- α measurements (Pryor et al. 2003).

Lallement et al. (1985b) performed an analysis of Prognosz 5 and 6 measurements by comparing the model results with the varying “a” parameter that is responsible for the anisotropy of the solar wind. It was shown that the best agreement between the data and the model is achieved for a 30–50 % decrease in the ionization rate over the solar pole in comparison with the equatorial plane. The anisotropy of the total ionization was studied in much more details by the SOHO/SWAN instrument (e.g. Bertaux et al. 1997, 1999). Studies of the total ionization rate variations with latitude and solar cycle were also performed by Pryor et al. (2003).

It follows from the classical hot model that due to net effects of solar gravitation, radiation pressure, charge exchange and photoionization, the velocity distribution of the interstellar atoms are disturbed at about 15–20 AU in the upwind direction. In the downwind direction the “solar imprints” remain up to ~ 100 AU. A typical interstellar atom with a velocity of 20 km/s travels about 4 AU per year. The time which is needed for the atom to pass through the region where the ionization and gravitational effects are significant is therefore comparable with the 11 year solar cycle. Since the solar radiation and solar wind flux both change during the solar cycle, calculating the time-dependent variation of interstellar atoms within the heliosphere requires that both be taken into account (Blum et al. 1993; Kyrölä et al. 1994; Bzowski and Ruciński 1995; Ruciński and Bzowski 1995; Summanen 1996; Bzowski et al. 1997, 2002; Pryor et al. 2003; Quémerais et al. 2006).

The variability of the solar factors exerts a significant influence on the hydrogen density distribution within 10–20 AU from the Sun and is the most pronounced in the downwind region. [Ruciński and Bzowski \(1995\)](#) have modeled the number density of interstellar hydrogen in the frame of a time-dependent hot model. It was shown that the departures of the density profiles from the stationary model at different phases of the solar cycle are clearly visible up to 5 AU on the upwind side (approximately the same occurs in the sidewind direction) and to 15 AU in the downwind region. Further away from the Sun, the differences decrease and practically vanish beyond 15–20 AU in the upwind and 50–60 AU in the downwind directions, respectively.

[Bzowski and Ruciński \(1995\)](#) calculated the distributions of the H atom number density by using a number of stationary models with “instantaneous” values of the radiation pressure and ionization rate for the considered phase of the solar cycle. Comparison of these distributions with the results of non-stationary model has shown significant differences. Therefore, a time-dependent approach is essential to accurately model the interstellar H atoms within the heliosphere.

It is clear from the historical review above that the development of the models of the interstellar atoms inside the heliosphere is closely connected with the measurements of the backscattered solar Lyman- α radiation, and the requirements of the data analysis stimulated the theoretical model development.

It is important to underline that all of the models described above assume that interstellar atoms have a pristine interstellar Maxwellian distribution function before they start to interact with the heliosphere. However, by the 1970s ([Wallis 1975](#)) it was realized that before penetrating inside the heliosphere, interstellar atoms of hydrogen pass through the so-called heliospheric interface that is the region of the solar wind interaction with the charged component of the local interstellar medium. At the present time, there is no doubt that the neutral and plasma components interact in the heliospheric interface by charge exchange, and these components should be treated self-consistently in the models by taking into account their mutual interactions.

The Solar Wind/Local Interstellar Medium Interaction

The heliosphere as a circumsolar volume where the properties of the medium are primarily controlled by the Sun was first conceptualized by [Davis \(1955\)](#) prior to both Parker’s theoretical prediction of the existence of the solar wind ([Parker 1958](#)) and its discovery ([Gringauz et al. 1960](#); [Neugebauer and Snyder 1962](#)). According to the current paradigm, the boundary of the heliosphere is located at a distance of ~ 90 – 300 AU (where AU is the astronomical unit, or the distance from the Sun to the Earth, equal to 149.6 million kilometers). The nature and position of this boundary, as well as the structure and properties of the outer heliosphere, are governed by the interaction between the solar wind and the interstellar environment of the Sun. At present, there is no doubt that the Sun is moving inside the Local Interstellar Cloud (LIC), one of several very diffuse interstellar cloudlets found in the vicinity of the Sun ([Lallement 2001](#)). These cloudlets (also called the Local

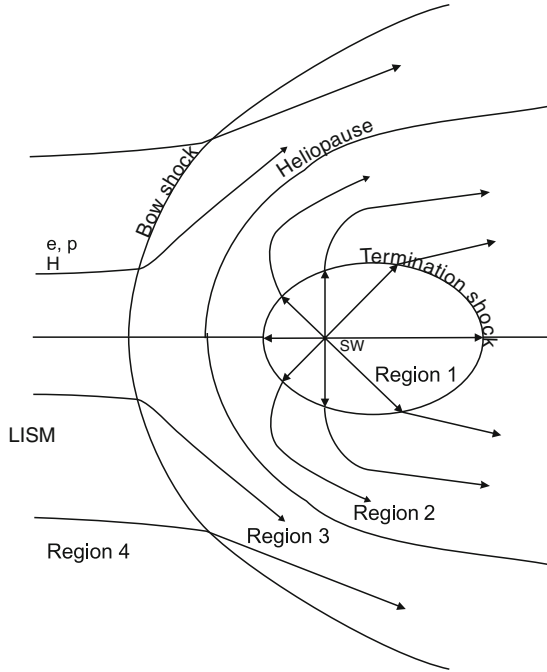


Figure 2.2: Qualitative picture of the SW interaction with the LIC. The *helopause* (HP) is a contact (or tangential) discontinuity which separates the solar wind plasma and the interstellar plasma component. The *termination shock* (TS) is formed due to the deceleration of the supersonic solar wind. The *bow shock* (BS) may also exist if the interstellar plasma flow is supersonic. Four regions are distinguished: the supersonic solar wind (region 1); the solar wind flow between the TS and the HP (region 2 or the *inner heliosheath*); the disturbed interstellar plasma component flow (region 3 or the *outer heliosheath*); the undisturbed interstellar gas flow (region 4)

Fluff) are in turn embedded in the Local Bubble that is believed to be made of hot ($\sim 10^6$ K) and tenuous ($\sim 10^{-3} \text{ cm}^{-3}$) gas with a characteristic size on the order of 100 pc (Welsh 2009).

The LIC is partially ionized (Lallement 2001). Interaction of the charged component of the LIC with the solar wind plasma gives rise to the formation of the interaction region, which is often called the *heliospheric interface* or *heliosheath* (Fig. 2.2). The heliospheric interface has a complex structure, where the solar wind and interstellar plasma, interplanetary and interstellar magnetic fields, interstellar atoms of hydrogen, galactic and anomalous cosmic rays (GCRs and ACRs) and pickup ions play important roles.

To get some insight into the structure and the physical processes inside the interface using remote observations, a theoretical model must be employed.

Theoretical studies of the heliospheric interface have been performed for more than four decades, following the pioneering work by [Parker \(1961\)](#) and [Baranov et al. \(1971\)](#). However, a complete theoretical model of the heliospheric interface has not yet been constructed. The basic difficulty stems from the multi-component nature of both the LIC and the solar wind. The LIC consists of at least four main components: plasma (electrons and protons), hydrogen atoms, interstellar magnetic field and galactic cosmic rays. The heliospheric plasma consists of particles of solar origin (protons, electrons, alpha particles, etc.), pickup ions and energetic particle components that include, for example, the termination shock particles (TSP) ([Stone et al. 2005](#); [Decker et al. 2005](#); [Burlaga et al. 2005](#)) and the anomalous cosmic ray (ACR) component. Pickup protons (or ions) are created by processes of charge exchange, photoionization and electron impact ionization, and after being ionized immediately picked up by the magnetic field. The pickup protons modify the heliospheric plasma flow starting from $\sim 20\text{--}30$ AU from the Sun. TSPs and ACRs may also modify the plasma flow upstream of the termination shock and in the heliosheath.

The first self-consistent stationary model of the interaction of the two-component (plasma and H atoms) LIC with the solar wind was developed by [Baranov and Malama \(1993\)](#). The interstellar wind was assumed to be an homogeneous parallel supersonic flow, and the solar wind was assumed to be spherically symmetric at Earth's orbit. Under these assumptions, the heliospheric interface has an axisymmetric structure. The main physical process of this interaction is resonance charge exchange (H atoms with protons), although the processes of photoionization and ionization of H-atoms by electron impact can be important in some regions of the heliosphere (for example, in the inner heliosheath or in the supersonic solar wind). The significant effect of the resonance charge exchange is connected with the large cross section of such collisions that is a function of the relative velocity of colliding particles. However, it was discussed by some authors ([Williams et al. 1997](#)) that elastic H-H and H-proton collisions can be important in the problem of the solar wind interaction with the local interstellar medium. This specific question was discussed in detail by [Izmodenov et al. \(2000\)](#) and it was shown that the elastic collisions are negligible.

The first self-consistent model of the SW/circumheliospheric interstellar medium (CHISM) interaction was developed by [Baranov and Malama \(1993\)](#). This is an axisymmetric and stationary two-component model. The plasma component is quasi-neutral and consists of electrons and protons. It is assumed that pickup protons are assimilated into the plasma component immediately after ionization. The plasma component is described as a fluid, and the Euler equations are solved to get the spatial distribution of the plasma number density, $n_p(\mathbf{r})$, bulk velocity, $\mathbf{V}_p(\mathbf{r})$, and pressure $P_p(\mathbf{r})$. The neutral component consists of hydrogen atoms and is described kinetically. The two components interact by charge exchange. Photoionization and electron impact ionization are taken into account in the model as well.

The main results of the model can be described as follows. The interstellar atoms strongly influence the heliospheric interface structure. The heliospheric

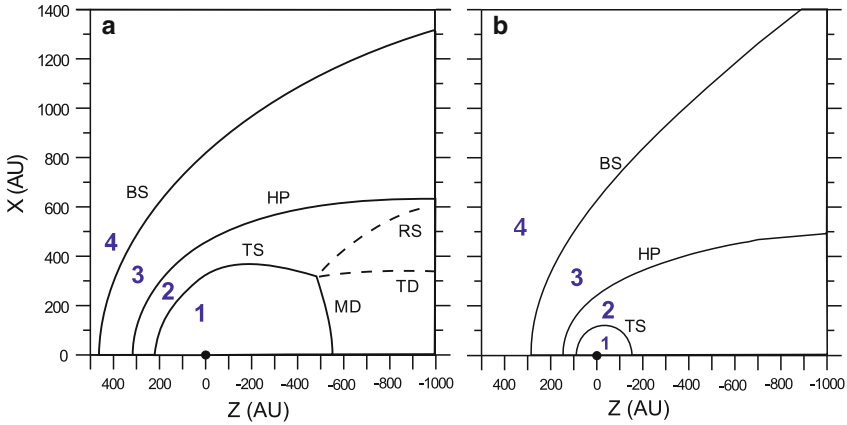


Figure 2.3: Effect of the interstellar H atoms on the geometrical pattern of the interface. (a) The heliospheric interface pattern in the case of a fully ionized circum-heliospheric interstellar medium (CHISM), (b) the case of partly ionized CHISM. Here BS, HP, and TS are the bow shock, the heliopause and the termination shock, respectively. MD and TD are the Mach disk and the tangential discontinuity; RS is the reflected shock that is formed in the case of a fully ionized plasma. These results were obtained initially by Baranov and Malama (1993). Region 1 is the supersonic solar wind, 2 is the inner heliosheath between the TS and HP, 3 is the outer heliosheath between the HP and BS [From Izmodenov and Alexashov (2003)]

interface is much closer to the Sun in the case when the H atoms are taken into account in the model as compared to the pure gas dynamical case as shown in Fig. 2.3.

The termination shock becomes more spherical and the flow in the region between HP and TS becomes subsonic (the sonic lines disappear). The Mach disk and the complicated tail shock structure, consisting of the reflected shock (RS) and the tangential discontinuity (TD), disappear as well.

The supersonic flows upstream of the bow and termination shocks are modified due to charge exchange with the neutral component. The supersonic solar wind flow (region 1 in Fig. 2.3) is modified by charge exchange with the interstellar neutrals. The new protons created by charge exchange are picked up by the solar wind magnetic field. The Baranov–Malama model assumes immediate assimilation of the pickup ions into the solar wind plasma. The solar wind protons and pickup protons are treated as one-fluid, called the solar wind. The number density, velocity, temperature, and Mach number of the solar wind are shown in Fig. 2.4a.

The effect of charge exchange on the solar wind is significant. By the time the solar wind flow reaches the termination shock, it is decelerated by 15–30 %, heated by a factor of 5–8, and loaded with the pickup proton component (approximately 20–50 %).

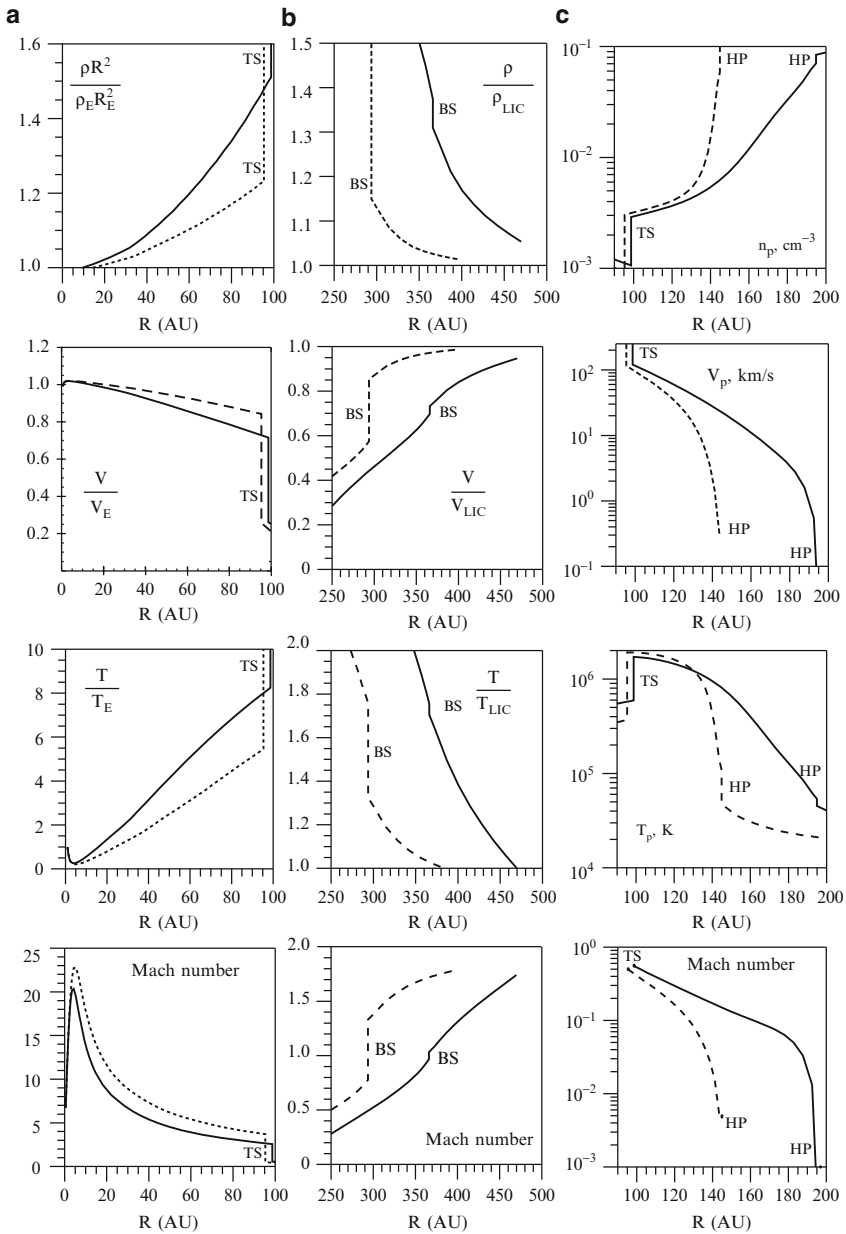


Figure 2.4: Plasma density, velocity, temperature, and Mach number upstream of the termination shock (a), upstream of the bow shock (b), and in the heliosheath (c). The distributions are shown for the upwind direction. The solid curves correspond to $n_{H,CHISM} = 0.2 \text{ cm}^{-3}$, $n_{p,CHISM} = 0.04 \text{ cm}^{-3}$. The dashed curves correspond to $n_{H,CHISM} = 0.14 \text{ cm}^{-3}$, $n_{p,CHISM} = 0.10 \text{ cm}^{-3}$. $V_{CHISM} = 25.6 \text{ km/s}$ and $T_{CHISM} = 7,000 \text{ K}$ in both cases [From [Izmodenov \(2000\)](#)]

The interstellar plasma flow is modified upstream of the bow shock by charge exchange between the interstellar protons and secondary H atoms. These secondary atoms originate in the solar wind. This leads to heating (40–70 %) and deceleration (15–30 %) of the interstellar plasma before it reaches the bow shock (BS). The Mach number decreases upstream of the BS and for a certain range of interstellar parameters ($n_{\text{H,CHISM}} \gg n_{\text{p,CHISM}}$) the bow shock may disappear. The solid curves in Fig. 2.4b correspond to a small degree of ionization in the CHISM ($n_{\text{p}}/(n_{\text{p}} + n_{\text{H}}) = 1/6$); the bow shock almost disappears in this case.

The interstellar neutrals also modify the plasma structure in the inner heliosheath. In a pure gasdynamic case (without neutrals) the density and temperature of the postshock plasma are nearly constant. However, the charge exchange process leads to a large increase in the plasma number density and decrease in its temperature (Fig. 2.4c). The electron impact ionization process may influence the heliosheath plasma flow by increasing the gradient of the plasma density from the termination shock to the heliopause (HP, Baranov and Malama 1996). The influence of interstellar atoms on the heliosheath plasma flow is important, in particular, for the interpretation of kHz-radio emissions detected by Voyager and for analysis of the heliospheric ENA fluxes.

Charge exchange significantly alters the interstellar atom flow. The atoms newly created by charge exchange have the velocity of their ion counterparts in the charge exchange collisions. Therefore, the velocity distribution of these new atoms depends on the local plasma properties in the location of their origin. It is convenient to distinguish four different populations of atoms, depending on the region in the heliospheric interface where the atoms were formed. Population 1 are the atoms created in the supersonic solar wind up to the TS (region 1 in Fig. 2.3), population 2 are the atoms created in the inner heliosheath (region 2 in Fig. 2.3), and population 3 are the atoms created in the outer heliosheath (region 3 in Fig. 2.3). The atoms of population 3 are often called the secondary interstellar atom component. We will refer to the original (or primary) interstellar atoms as population 4. The number densities and mean velocities of these populations are shown in Fig. 2.5I as functions of heliocentric distance. The distribution function of H atoms, $f_{\text{H}}(\mathbf{r}, \mathbf{w}_{\text{H}})$, can be represented as a sum of the distribution functions of these populations: $f_{\text{H}} = f_{\text{H},1} + f_{\text{H},2} + f_{\text{H},3} + f_{\text{H},4}$. The Monte Carlo method allows us to calculate these four distribution functions. These distributions were presented by Izmodenov (2001) and Izmodenov et al. (2001) at 12 selected points in the heliospheric interface. As an example, the distribution functions at the termination shock in the upwind direction are shown in Fig. 2.5II for the four introduced populations of H atoms. It is seen from this figure that the distribution functions of all H-atom populations are not Maxwellian inside the heliosphere, i.e. the fluid approach is not correct for describing the motion of neutral atoms. Comparisons of kinetic and different multi-fluid approaches show significant differences in the results (Izmodenov and Alexashov 2005; Mueller et al. 2008).

Original (or primary) interstellar atoms (population 4) are significantly filtered (i.e. their number density is reduced) before reaching the termination shock (Fig. 2.5I-a). The outer heliosheath is the main “filter” for these atoms. Since the slow atoms have a small mean free path (due to both larger charge exchange cross sections and smaller velocities) in comparison with the fast atoms, they suffer larger

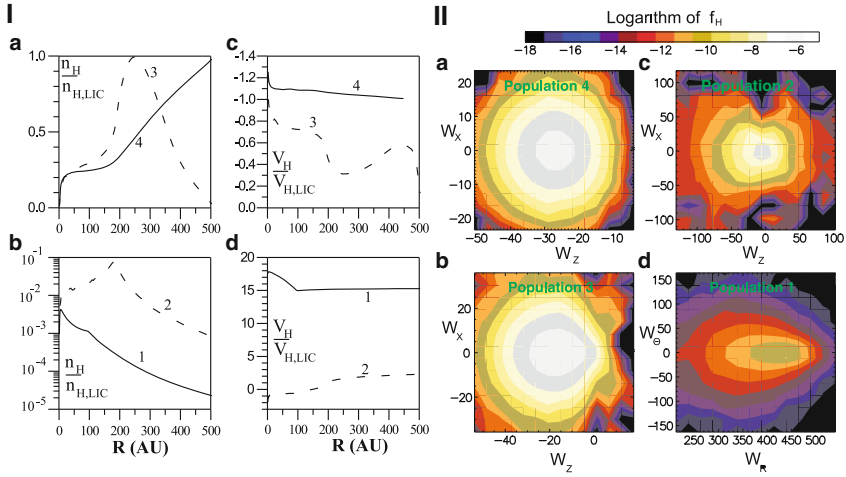


Figure 2.5: **I.** Number densities and velocities of the four atomic populations as functions of heliocentric distance in the upwind direction. 1 designates atoms created in the supersonic solar wind, 2 atoms created in the heliosheath, 3 atoms created in the disturbed interstellar plasma, and 4 original (or primary) interstellar atoms. Number densities are normalized to $n_{H,CHISM}$, velocities are normalized to V_{CHISM} . It is assumed that $n_{H,CHISM} = 0.2 \text{ cm}^{-3}$, $n_{p,CHISM} = 0.04 \text{ cm}^{-3}$. **II.** Velocity distributions of the four atom populations—primary interstellar atoms (population 4), secondary interstellar atoms (population 3), atoms created in the inner heliosheath (population 2), atoms created in the supersonic solar wind (population 1)—at the termination shock in the upwind direction; w_z is the projection of the velocity vector on the axis parallel to the LIC velocity vector. Negative values of w_z indicate approach to the Sun. w_x is the magnitude of the projection of the velocity vector on the plane perpendicular to the interstellar velocity vector; w_R, w_θ are radial and tangential velocity components. All velocities are in km/s [From Izmodenov et al. (2001)]

losses. This kinetic effect, called *selection*, results in a deviation of the interstellar distribution function from a Maxwellian (Fig. 2.5II-a). The selection also results in a $\sim 10\%$ increase in the primary atom mean velocity towards the termination shock (Fig. 2.5I-c).

Secondary interstellar atoms (population 3) are created in the disturbed interstellar medium by charge exchange between the primary interstellar neutrals and protons decelerated in the vicinity of the heliopause. The secondary interstellar atoms collectively make up the *hydrogen wall*, a density enhancement at the heliopause. The *hydrogen wall* was predicted by Baranov et al. (1991) and detected in the direction of α Cen (Linsky and Wood 1996) by the Hubble Space Telescope. At the termination shock, the number density of secondary neutrals is comparable to the number density of the primary interstellar atoms (Fig. 2.5I-a, dashed curve).

The relative abundances of secondary and primary atoms entering the heliosphere vary with the degree of interstellar ionization. The bulk velocity of population 3 is about $-18 \div -19$ km/s. The sign “-” means that the population approaches the Sun. One can see that the distribution function of this population is not Maxwellian (Fig. 2.5II-b). The reason for the abrupt behavior of the distribution function for $w_z > 0$ is that the particles with significant positive w_z velocities can reach the termination shock only from the downwind direction. The distribution functions of different H atom populations were calculated by [Izmodenov et al. \(2001\)](#) for various upwind directions. The fine structures of the distribution functions of the primary and secondary interstellar populations vary with direction. The directional variation of the velocity distribution reflects the geometrical pattern of the heliospheric interface. The distribution functions of the interstellar atoms can be a good diagnostic of the global structure of the heliospheric interface.

Another population (population 2) of the heliospheric hydrogen atoms are the atoms created in the inner heliosheath by charge exchange with hot and compressed solar wind and pickup protons. The number density of this population is by an order of magnitude smaller than the number densities of the primary and secondary interstellar atoms. This population has a minor importance for the interpretation of Lyman- α and pickup ion measurements inside the heliosphere. Some atoms of this population may probably be detectable by a Lyman- α hydrogen cell experiment due to their large Doppler shifts ([Quémerais and Izmodenov 2002](#)). Recently it was pointed out by [Chalov and Fahr \(2003\)](#) that charge exchange of these atoms with solar wind protons may produce tails in the distribution function of pickup ions that are measured at one or several AU from the Sun during quiet time periods. [Gruntman and Izmodenov \(2004\)](#) showed that this population of H-atoms is a major contributor to the density of interplanetary hydrogen at heliocentric distances < 1 AU and could dominate in the downwind (interstellar wind) region under typical solar and interstellar conditions. Mass transport by heliospheric ENAs may become especially important for determining the origin of the pickup ions attributed to the inner source of neutral particles in the Sun’s vicinity.

Due to their high energies and large mean free path, a portion of the atoms from this population penetrate upstream of the BS and modify the pristine interstellar medium at large heliocentric distances. These atoms propagate freely in the supersonic solar wind. Thus, these atoms are a rich source of information on the plasma properties at the place of their birth, i.e. at the inner heliosheath. This population of atoms is measured by the Interstellar Boundary Explorer (IBEX).

The last population of the heliospheric atoms are the atoms created in the supersonic solar wind (population 1). The number density of this atom population takes its maximum at ~ 5 AU. At this distance, the number density of the population is about two orders of magnitude smaller than the number density of interstellar atoms. Outside the termination shock the density decreases faster than r^{-2} , where r is the heliocentric distance (curve 1, Fig. 2.5I-b). The mean velocity of population 1 corresponds to the bulk velocity of the supersonic solar wind and is about 450 km/s. The distribution function of this population is also not Maxwellian (Fig. 2.5II-d). The extended “tail” in the distribution function is caused by the solar wind plasma deceleration upstream of the termination shock. This “supersonic” atom population penetrates the interface and charge exchanges

with interstellar protons beyond the BS. The process of charge exchange leads to heating and deceleration of the interstellar gas upstream of the bow shock and, therefore, to a decrease of the Mach number ahead of the bow shock.

Since 2003 the standard Baranov–Malama model has been modified by adding solar wind alpha particles and interstellar helium ions to plasma components (Izmodenov et al. 2003). Up to now, helium ions and alpha particles are not included in the alternative models of other groups.

To evaluate possible effects of both interstellar ions of helium and solar wind alpha particles, Izmodenov et al. (2003) performed parametric model calculations. It was shown that the heliopause and the termination and bow shocks, are closer to the Sun when the influence of interstellar helium ions is taken into account. This effect is partially compensated by additional solar wind alpha particle pressure that was also taken into account in the model. The net result is as follows: the heliopause, termination and bow shocks are closer to the Sun by ~ 12 AU, ~ 2 AU, ~ 30 AU, respectively in the model taking into account both interstellar helium ions and solar wind alpha particles as compared to the model ignoring these ionized helium components. Despite the fact that the net effect of interstellar helium ions and solar alpha particles is rather small ($\sim 7\%$ displacement for the heliopause, $\sim 10\%$ the BS, and $\sim 2\%$ for the TS), it still can be important for the interpretation and prediction of experimental data related to the inner heliosheath region.

Aleksashov et al. (2000) explored the problem of solar wind interaction with the CHISM for the case where the interstellar magnetic field is parallel to the relative Sun/CHISM velocity vector. In this case, the model remains axisymmetric. It was shown that the effect of the interstellar magnetic field on the positions of the TS, BS and HP is significantly smaller when H atoms are included (Baranov and Zaitsev 1995). The calculations were performed with various Alfvén Mach numbers in the undisturbed CHISM. It was found that the bow shock straightens out with decreasing Alfvén Mach number $M_A = V_{\text{CHISM}}\sqrt{4\pi\rho}/B_{\text{CHISM}}$ (i.e. with an increasing magnetic field strength in the CHISM). It gets closer to the Sun near the symmetry axis, but recedes from it on the flanks. By contrast, the nose of the heliopause recedes from the Sun due to the tension of magnetic field lines, while the wings of the heliopause get closer to the Sun due to magnetic pressure. As a result, the region of the compressed interstellar medium at the heliopause (or “pileup region”) is reduced by almost 30%, as the magnetic field increases from zero to 3.5×10^{-6} Gauss. It was also shown that the H atom filtration and heliospheric distributions of primary and secondary interstellar atoms are virtually unchanged over the entire considered range of the interstellar magnetic field (0 – 3.5×10^{-6} Gauss). The magnetic field has the strongest effect on the density distribution of population 2 of H atoms, which increases by a factor of almost 1.5 as the interstellar magnetic field increases from zero to 3.5×10^{-6} Gauss.

Izmodenov et al. (2005), as well as Izmodenov and Alexashov (2005, 2006), studied the problem assuming that the interstellar magnetic field (IsMF) is inclined with respect to the direction of the interstellar flow. In this case, the SW/CHISM interaction region becomes asymmetric and the flow pattern becomes essentially three-dimensional. Here we present new results obtained within the framework of this model for the interstellar magnetic field $B_{\text{CHISM}} = 4.4 \mu\text{G}$ and $\alpha = 15^\circ$, where α is the angle between the CHISM flow velocity and the IsMF direction.

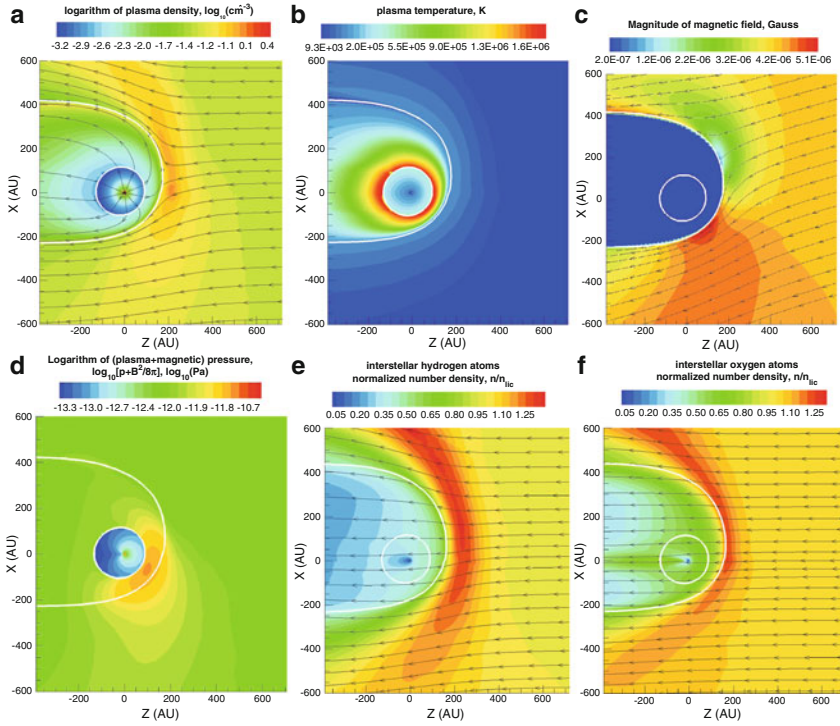


Figure 2.6: Isocontours of the proton number density (plot **a**), plasma temperature (plot **b**), magnetic field (plot **c**), total thermal plasma and magnetic pressure (plot **d**), normalized hydrogen (plot **e**) and oxygen (plot **f**) number densities in the plane determined by the interstellar velocity and magnetic field vectors. The streamlines of the plasma component (plot **a**), the magnetic field lines (plot **c**) and “streamlines” of the hydrogen (plot **e**) and oxygen (plot **f**) atoms are shown. The termination shock and heliopause are shown as white curves [From [Izmodenov et al. \(2009\)](#)]

Figure 2.6 shows the results of the model calculations in the xz plane. The xz plane is determined by the Sun-CHISM relative velocity vector and the interstellar magnetic field vector. The direction of the z -axis is chosen to be opposite to the interstellar gas velocity vector. The plasma streamlines and isolines of the plasma density are shown in panel **a**, the plasma temperature in panel **b**, and the total (plasma thermal plus magnetic field) pressure in panel **d**. Panel **c** shows the magnetic field lines and isocontours of the interstellar magnetic field. The heliopause and the termination shock become asymmetric with respect to the direction of the interstellar flow due to the asymmetric pressure of the IsMF (panel **c**).

The interstellar magnetic field pressure pushes the heliopause and the termination shock towards the Sun as compared to the model without magnetic field.

Table 2.1: Positions of the TS in the directions of Voyager 1 and Voyager 2

B	0	2.5	2.5	5.0	4.375	4.375	2.5	2.5	1.25	2.5	2.5
$\alpha(B, V)$		0	15	15	15	20	30	45	45	60	90
Cross section	MT	MT	MT	MT	Steb.	Steb	MT	MT	MT	MT	MT
V1	98	99.9	97.4	92.2	96.0	93.3	91.5	85.8	92.1	84.5	83.1
V2	98	99.7	94.2	82.3	86.5	82.4	87.6	82.5	90.6	82.2	83.2

B is B_{CHISM} , and $\alpha(B, V)$ is $\alpha(B_{\text{CHISM}}, V_{\text{CHISM}})$. MT uses the charge-exchange cross-section from [Maher and Tinsley \(1977\)](#), while Steb indicates the charge-exchange cross-section from [Lindsay and Stebbing \(2005\)](#)

Quantitatively the effect of the IsMF on the location of the TS in the directions of Voyager 1 and Voyager 2 is shown in Table 2.1. The TS distances in this table are obtained in the framework of the stationary 3D kinetic-MHD model that is under discussion, but corrected according to a kinetic-gasdynamic model of the interface by [Izmodenov et al. \(2008\)](#) that takes into account solar cycle effects ([Izmodenov 2009](#)). It is seen from the table that the models with $B_{\text{CHISM}} = 4.375 \mu\text{G}$ and $\alpha = 15^\circ\text{--}20^\circ$ are in good agreement with the actual distances of 94 AU and 84 AU of the Voyager 1 and 2 crossings of the TS. This is the reason why this model is presented here. It is interesting to note that using a multi-fluid approach for interstellar H atoms allows us to estimate the distances for comparable observations in other directions of the interstellar magnetic field and not just in the directions measured by the Voyagers ([Opher et al. 2009](#)). The detailed discussion and comparison with models of other groups is out of the scope of the paper ([Izmodenov and Alexashov 2005](#)).

The bow shock disappears for such a strong magnetic field because the Mach numbers calculated with respect to the Alfvén and fast magnetosonic waves are smaller than one.

Figure 2.6a also shows the streamlines of the plasma component. The stagnation point is located in the upper half of the zx plane and is displaced from the z axis. It is important to note that the velocity vector of the plasma passing through the region of maximum plasma density has a noticeable V_x component. The secondary interstellar atoms which originate in the vicinity of the HP should have the properties of the plasma in this region. Figure 2.6e presents the number density of this interstellar atom component. The maximum density appears in the region between the HP and the BS. This is the so-called hydrogen wall, as discussed above. It is seen in the figure that the maximum of the hydrogen wall is also slightly shifted to the upper half of the xz plane and reflects the behavior of the plasma distributions. The streamlines of the H atom component are also shown in Fig. 2.6e. The streamlines were plotted based on the mean velocity field distribution of the interstellar H atoms. The velocity vector \mathbf{V}_H determines the direction of the averaged H atom flow. It can be seen from the figure that in the heliosphere the velocity vector \mathbf{V}_H has a noticeable V_x component even very close to the Sun. The effect of the shift of the direction of interstellar hydrogen flow relative to the direction of the interstellar helium flow was observed by the SOHO/SWAN H cell instrument ([Lallement et al. 2005](#)).

The measurements of the deflection of the interstellar H atom flow relative to the direction of the interstellar helium flow is one of several observational constraints on the magnitude and direction of the interstellar magnetic fields. Estimates performed by [Izmodenov et al. \(2005\)](#) and [Izmodenov and Alexashov \(2006\)](#) showed that the models with $B_{\text{CHISM}} = 2.5 \mu\text{G}$, and $\alpha = 30 - 45^\circ$ provide levels of deviation in agreement with the level obtained from analysis of the SOHO/SWAN data. However, recent numerical results ([Alexashov et al. 2008](#)) showed that the deflection angle is very sensitive to the charge exchange cross section. Results of calculations with updated cross section from [Lindsay and Stebbing \(2005\)](#) show a larger deflection angle as compared with the previous calculations which employed the cross section from [Maher and Tinsley \(1977\)](#).

Other possible constraints on the direction and magnitude of the interstellar magnetic field are:

1. Asymmetries of the TS toward Voyager 1 and Voyager 2 direction, which were discussed before
2. Flows of the solar wind beyond the TS that are directly measured by Voyager 2 ([Opher et al. 2009](#)) and estimated from the anisotropy of the energetic particle fluxes from Voyager 1 ([Krimigis et al. 2011](#))
3. Analyses of the heliospheric ENA fluxes measured by IBEX ([Heerikhuizen and Pogorelov 2011](#)).

More detailed parametric model calculations are required and the work is currently in progress.

The Baranov–Malama model and more recent models described above assume immediate assimilation of pickup protons into the solar wind plasma and consider the mixture of solar wind and pickup protons as a single component.

However, measurements of the pickup proton distribution function on board the Ulysses and ACE spacecraft show that the pickup proton distribution function is non-Maxwellian. The observations show also that the velocity distribution function can be considered as isotropic (fast pitch-angle scattering) except some short periods in the inner heliosphere when the interplanetary magnetic field is almost radial. These data point to the absence of thermodynamic equilibrium between the pickup and solar-origin protons, although their mean velocities are equal. In the improved model of the solar wind/interstellar medium interaction developed by [Malama et al. \(2006\)](#), the pickup protons are considered as a separate component with thermodynamic parameters different from those of the solar wind. Since in the solar-wind reference frame, the pickup proton distribution function is assumed to be isotropic, the following angle-averaged distribution function can be introduced:

$$f_{\text{pui}}^*(\mathbf{r}, w) = \frac{1}{4\pi} \int \int f_{\text{pui}}(\mathbf{r}, \mathbf{v}) \sin \theta d\theta d\phi. \quad (2.2)$$

Here, \mathbf{v} is the individual velocity of a pickup proton, $\mathbf{w} = \mathbf{v} - \mathbf{V}$ is the pickup proton velocity in the solar-wind reference frame (\mathbf{V} is the solar wind velocity in the heliocentric coordinate system), w , θ , and ϕ are the spherical coordinates of vector \mathbf{w} , and $f_{\text{pui}}(\mathbf{r}, \mathbf{v})$ is the pickup proton distribution function. The kinetic

equation for $f_{\text{pui}}^*(\mathbf{r}, w)$ can be written in the form (Isenberg 1987):

$$\frac{\partial f_{\text{pui}}^*}{\partial t} + \mathbf{V} \cdot \frac{\partial f_{\text{pui}}^*}{\partial \mathbf{r}} = \frac{1}{w^2} \frac{\partial}{\partial w} \left(w^2 D \frac{\partial f_{\text{pui}}^*}{\partial w} \right) + \frac{w}{3} \frac{\partial f_{\text{pui}}^*}{\partial w} \text{div} \mathbf{V} + S(\mathbf{r}, w). \quad (2.3)$$

Here, $D(\mathbf{r}, w)$ is the diffusion coefficient in the velocity space, while the source function of pickup protons $S(\mathbf{r}, w)$ reflects their birth and loss due to charge exchange, photoionization, and the electron impact ionization of H atoms. Malama et al. (2006) assumed for simplicity that $D(\mathbf{r}, w) = 0$ and the kinetic equation (2.3) was solved together with the Euler equations written for the sum of all the charged components and the kinetic equation for the interstellar hydrogen atoms. The use of Euler equations for the sum of the charged components is justified by the fact that all the components (solar protons and electrons, as well as pickup protons) move at the same velocity and that for all the components the distribution functions are isotropic. In this case, the pressure p is equal to the sum of partial pressures, while the effective pressure of the pickup protons is determined in terms of the distribution function f_{pui}^* , so that:

$$p = p_e + p_p + p_{\text{pui}}, \quad p_{\text{pui}} = \frac{4\pi}{3} \int m_p w^4 f_{\text{pui}}^*(\mathbf{r}, w) dw$$

To treat the passage of pickup protons through the termination shock we assume the conservation of their magnetic moment. The analytical derivation of the magnetic moment conservation has been done by Alekseev and Kropotkin (1971) for perpendicular and nearly perpendicular shocks. Later it has been shown numerically by Terasawa (1979) that the conservation of the magnetic moment exists for all quasi-perpendicular shocks.

The reflections of pickup protons at the shock potential is not taken into account. A self-consistent solution of the problem just formulated was obtained by Malama et al. (2006) for the case $D = 0$ corresponding to a quiescent solar wind in which the magnetic field fluctuation level is low.

The thermodynamic non-equilibrium of the pickup and solar protons leads to a thinning of the inner heliosheath region (Fig. 2.7a), which is attributable to the decrease in the total pressure of the charged component. As compared with the calculations performed in accordance with the corresponding equilibrium model, the TS is displaced by 5 AU away from the Sun in the direction of the oncoming flow, whereas the HP is by 12 AU closer. In the tail region, the heliocentric distance of the TS increases by 70 AU.

Recently we expanded the Malama et al. (2006) model by including the pickup proton component outside the heliopause. Indeed, energetic hydrogen atoms which originated in the supersonic solar wind and the inner heliosheath can penetrate through the heliopause and enter into the interstellar plasma. Outside the heliopause the atoms can suffer charge exchange with interstellar protons. As a result new energetic interstellar pickup protons are created. Having an energy of 1 keV or more, these pickup protons have large mean free path as compared with the thermal interstellar protons and can be considered as collisionless with a non-Maxwellian velocity distribution. The pickup protons in the outer heliosheath can charge exchange with interstellar H atoms. Eventually, new ENAs of the outer

heliosheath origin will be created in this secondary charge exchange. Similar to the ENAs from the inner heliosheath, the ENAs originating in the outer heliosheath can penetrate to small heliocentric distances and be measured there.

Figure 2.7b shows the calculated fluxes of H atoms at 1 AU obtained within the framework of the new non-equilibrium model. The figure presents total fluxes of all heliospheric ENAs (solid curve), fluxes of ENAs originated in the inner heliosheath from solar wind protons (black dots), fluxes of the ENAs originated in the inner heliosheath from the pickup protons (blue triangles), and fluxes of the ENAs originated in the outer heliosheath from the pickup protons (blue dots). The ENAs originated in the inner heliosheath from the solar wind protons are the strongest at energies of ~ 0.02 – 0.2 keV. For this energy range the fluxes of the ENAs from the outer heliosheath (blue dots in Figure) are smaller but still comparable. In the energy range of ~ 0.4 – 1.0 keV the ENAs originating in the inner heliosheath from the pickup protons (blue triangles in Figure) dominate, while for energies above 2 keV fluxes of the ENAs from the outer heliosheath (blue dots) become higher than the other. Therefore, the model suggests that the ENAs with energies above 1 keV may be of interstellar (outer heliosheath) origin. The ENAs of such energies have been measured on board of several spacecraft. Upper limits of the heliospheric ENA fluxes estimated from measurements on board of SOHO/CELIAS (Hilchenbach et al. 1998; Hilchenbach et al. 2000), Cassini/INCA (Krimigis et al. 2009) and Venus Express (Brandt et al. 2009) are shown in Fig. 2.7b as green dots. The figure shows that generally there is a good agreement between the model results and the data.

Here we should also note that the calculations were performed in the framework of a model that has no stochastic mechanisms for pickup proton acceleration (Malama et al. 2006). Izmodenov et al. (2009) presented an extension of the Malama et al. (2006) model by introducing a non-thermal population of pickup protons in the interstellar medium. It has been shown that the interstellar pickup protons form significant fluxes of ENAs due to charge-exchange, and those fluxes exceed the fluxes of other ENAs at energies above ~ 1 keV. These models predict that the ENA fluxes have maxima near the upwind direction of the heliosphere and minima at the flanks, though, of course, the position of the maxima can slightly deviate from the upwind direction due to the effects of the interstellar magnetic field and SW asymmetry (Izmodenov et al. 2009).

The first full sky maps of heliospheric ENAs measured by the Interstellar Boundary Explorer (IBEX) spacecraft (McComas et al. 2009; Fuselier et al. 2009; Funsten et al. 2009; Schwadron et al. 2009) show results that were entirely unexpected in the frame of the previously discussed models. The first scan of the whole sky showed that maxima of ENA fluxes form a long ($\sim 250^\circ$ – $\sim 300^\circ$) and narrow arc-like feature called ribbon that was not predicted by any model prior to the IBEX observations. Chalov et al. (2010) proposed a modification of the Malama et al. (2006), Izmodenov et al. (2009) model that ignore the scattering of newly created energetic pickup protons, but including the effects of ion transport for the pickup protons generated in the region outside of the heliopause by charge exchange between the thermal interstellar protons and heliospheric ENAs. The results of the

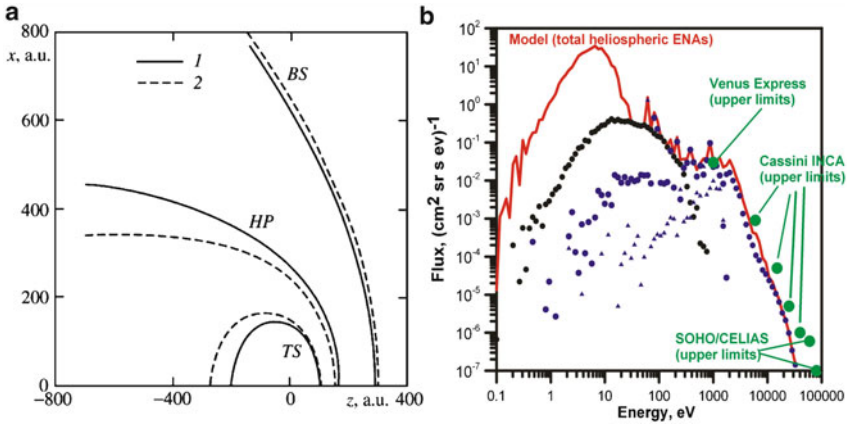


Figure 2.7: (a) Strong discontinuity surfaces calculated taking into account the pickup proton non-equilibrium (curves 1), and in accordance with the equilibrium plasma model (curves 2). (b) Fluxes of H atoms at 1 AU calculated with the pickup proton non-equilibrium model: total fluxes of all heliospheric ENAs (*solid curve*), ENAs originated in the inner heliosheath from solar wind protons (*black dots*), ENAs originated in the inner heliosheath from pickup protons (*blue triangles*), ENAs originated in the outer heliosheath from pickup protons (*blue dots*). Upper limits of the heliospheric ENA fluxes measured by SOHO/CELIAS, Cassini/INCA and Venus Express are shown by the *green dots* [From Izmodenov et al. (2009)]

model yield a feature qualitatively similar to the IBEX ribbon. In future studies, the results of simulations will be quantitatively compared to the IBEX ENA observations.

Note, however, that the more complex kinetic description of the supra-thermal population of pickup protons has no direct influence on the primary and secondary populations of the interstellar atoms which are created from the thermal protons of the interstellar plasma. Nevertheless, an indirect influence is possible because taking into account the pickup component properly would change the thermal population too. Therefore, we do not expect that the effects of the non-equilibrium plasma model would dramatically change the previous conclusion on the properties of the primary and secondary interstellar atoms, but some effects are possible mainly due to global dynamic effects (Malama et al. 2006) and need to be checked in future.

Summary of the Section

This section reviewed a modern state of the art in the kinetic-MHD models of the solar wind interaction with the local interstellar medium developed by the Moscow group (Baranov and Malama 1993). The multi-component and non-equilibrium nature of both the solar wind and LISM requires development of

complex 3D kinetic-MHD models of the SW/LIC interaction region. The most important aspect of the model for the purpose of this paper is that upon entering the heliosphere, the distribution function of interstellar H atoms is strongly disturbed in the SW/LIC interaction region. This means that the properties of the interstellar atoms inside the heliosphere are dependent on the structure of the heliospheric interface, and, therefore, the distribution function of interstellar hydrogen can not be used directly to determine the local interstellar parameters as it would be if the population of these atoms were not disturbed in the heliospheric interface. At the same time, this opens up a possibility to use the backscattered solar Lyman- α radiation as a diagnostic of the properties of the heliospheric interface.

Advanced Model of the Interstellar Hydrogen in the Heliosphere

Recently, [Katushkina and Izmodenov \(2010, 2011\)](#) developed a model that allows to combine simplicity of the hot-type models of the H atom distribution inside the heliosphere with the results of the global models of the SW/LIC interaction. Briefly the model can be classified as a time-dependent 3D version of a classical hot model with the boundary conditions at 90 AU taken from the global models of the SW/LIC interaction. This section describes this model and presents some results including both the global effects of the heliospheric interface and the three-dimensional and time-dependent local effects in the vicinity (2–10 AU) of the Sun.

Description of the Model

Our advanced model describes the velocity and spatial distribution of interstellar hydrogen inside the heliospheric termination shock. The effects of the SW/LIC interaction are taken into account in the boundary conditions, which are chosen at a sphere of radius 90 AU, centered at the Sun (see Fig. 2.8).

We consider only those atoms that penetrate into the heliosphere through the heliopause, i.e. the primary and secondary interstellar atoms (atoms of populations 4 and 3). Atoms created by charge exchange in the inner heliosheath (population 2) or in the supersonic solar wind (population 1) are neglected here. Neutral solar wind (population 1) is not important for backscattering solar Lyman- α photons, because of their small number densities and a large Doppler-shift beyond the spectral range of the Lyman- α line. Backscattered Lyman- α from the atoms of population 2 has been estimated by [Quémerais and Izmodenov \(2002\)](#). It has been shown that at the Earth orbit, the hot component of the backscattered intensity represents less than 5% of the total intensity in the upwind direction. It reaches 15% in the downwind direction. Due to relatively small importance we neglect the population 2 in this section, but it can be added later without any further modification in the model.

The solar gravitational force \mathbf{F}_g and solar radiation pressure \mathbf{F}_{rad} influence the motion of an atom inside the heliosphere. These forces counteract each other and are proportional to $1/r^2$. The total force acting on an atom is:

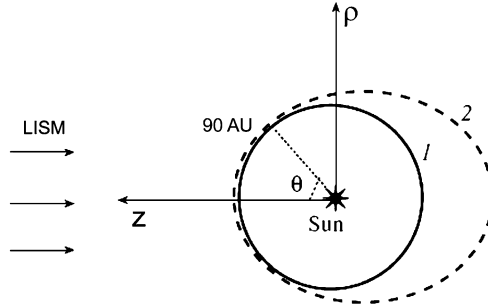


Figure 2.8: Coordinate system used in the axisymmetric models: z is the axis of symmetry directed toward the upwind direction, ρ is an axis in cylindrical coordinate system that is perpendicular to the upwind direction; curve 1 is the outer boundary in the advanced model of hydrogen distribution inside the heliosphere; curve 2 is a schematic representation of the heliospheric termination shock [From [Katushkina and Izmodenov \(2011\)](#)]

$$\mathbf{F}(\mathbf{r}) = m_H(1 - \mu)\mathbf{F}_g = -m_H \frac{(1 - \mu)GM_s}{r^2} \cdot \frac{\mathbf{r}}{r},$$

G is the gravitational constant, M_s the mass of the Sun, m_H the mass of a H atom, and \mathbf{r} the radius-vector to a point. μ is the ratio of gravitational attraction to repulsion from radiation pressure as defined in Eq. 2.1. In general, the parameter μ depends on time (t), heliolatitude (λ) and the radial component of velocity (w_r).

The kinetic equation for the velocity distribution function of H atoms can be written as:

$$\begin{aligned} \frac{\partial f(\mathbf{r}, \mathbf{w}, t)}{\partial t} + \mathbf{w} \cdot \frac{\partial f(\mathbf{r}, \mathbf{w}, t)}{\partial \mathbf{r}} + \\ \frac{\mathbf{F}(\mathbf{r}, t, \lambda, w_r)}{m_H} \cdot \frac{\partial f(\mathbf{r}, \mathbf{w}, t)}{\partial \mathbf{w}} = -\beta(r, t, \lambda) \cdot f(\mathbf{r}, \mathbf{w}, t) \end{aligned} \quad (2.4)$$

Here $f(\mathbf{r}, \mathbf{w}, t)$ is velocity distribution function of the hydrogen atoms, \mathbf{w} is the individual velocity of a H atom.

The right hand side of Eq. (2.4) represents losses of atoms due to charge exchange ($H + H^+ \leftrightarrow H^+ + H$) and photoionization ($H + h\nu = H^+ + e$). Electron impact ionization is not taken into account. The coefficient $\beta(r, t, \lambda)$ is the effective ionization rate: $\beta(r, t, \lambda) = \beta_{ex}(r, t, \lambda) + \beta_{ph}(r, t, \lambda)$, where β_{ex} and β_{ph} are rates of charge-exchange and photoionization, respectively. It is assumed that these rates of ionization decrease with distance from the Sun as $\sim 1/r^2$ (where r is the heliocentric distance), since these values are proportional to the number density of the solar protons and flux of the solar photons, respectively. Therefore:

$$\beta(r, t, \lambda) = (\beta_{ex,E}(t, \lambda) + \beta_{ph,E}(t, \lambda)) \left(\frac{r_E}{r} \right)^2 = \beta_E(t, \lambda) \left(\frac{r_E}{r} \right)^2,$$

where $r_E = 1$ AU is the distance from the Earth to the Sun. The subscript E indicates that the values are measured at 1 AU.

The functions $\mu(t, \lambda, w_r)$, $\beta_{ex,E}(t, \lambda)$, and $\beta_{ph,E}(t, \lambda)$ adopted in this model are based on experimental data. Detailed descriptions of these functions will be given below.

The kinetic equation (2.4) is a linear partial differential equation, and it can be solved by the method of characteristics. It is known that the characteristics of this equation coincide with the trajectories of the atoms. The distribution function $f(\mathbf{r}, \mathbf{w}, t)$ changes along a characteristic according to the equation:

$$df(\mathbf{r}, \mathbf{w}, t)/dt = -\beta(r, t, \lambda) f(\mathbf{r}, \mathbf{w}, t).$$

The solution of the kinetic equation can then be obtained by integration of the last equation subject to boundary conditions:

$$f(\mathbf{r}, \mathbf{w}, t) = f_b(\mathbf{r}_0, \mathbf{w}_0, t_0) \exp\left(-\int_{t_0}^t \beta(r, t, \lambda) dt\right), \quad (2.5)$$

where $f_b(\mathbf{r}_0, \mathbf{w}_0, t_0)$ is the velocity distribution function of hydrogen atoms at the outer boundary (determined by the boundary conditions at 90 AU); $\mathbf{r}_0, \mathbf{w}_0, t_0$ are the position, velocity and time of the atom when the characteristic (i.e. the atom's trajectory) is crossing the outer boundary. The integration in the last equation is performed along the trajectory of the atom.

Kinetic Properties of the Hydrogen Distribution at 90 AU from the Sun

As was discussed in detail in the section “The Solar Wind/Local Interstellar Medium Interaction”, the velocity distribution function of interstellar hydrogen atoms is disturbed after they cross the heliospheric interface region. These disturbances occur mainly due to charge-exchange between primary interstellar atoms and decelerated and heated interstellar protons in the vicinity of the heliopause. As a result, the velocity distribution function of hydrogen is not Maxwellian at our outer boundary of 90 AU. In this section we will illustrate some kinetic non-Maxwellian features of the hydrogen distribution at 90 AU resulting from the Baranov–Malama (1993) model of the heliospheric interface. Since the model is axisymmetric, it is natural to use a cylindrical coordinate system as shown in Fig. 2.8, where the z -axis (upwind) is oriented towards the direction of the LIC flow, and the ρ -axis is perpendicular to the upwind direction (i.e. the crosswind direction). Also let us define the angular coordinate, θ , as positive in the clockwise direction.

In the frame of this axisymmetric model we can identify at least five features which will make the hydrogen velocity distribution function non-Maxwellian at 90 AU:

1. The existence of two populations of interstellar hydrogen atoms (primary and secondary), which are considerably displaced from each other in the velocity space (the secondary interstellar atoms have a smaller bulk velocity and a larger temperature as compared with the primary interstellar atoms).

2. Spatial inhomogeneity of the hydrogen distribution at 90 AU. All moments of the velocity distribution function (the number density, bulk velocity, and effective kinetic “temperatures”) strongly depend on θ .
3. Anisotropy of kinetic “temperatures”, i.e. $T_z \neq T_\rho$, where

$$T_z(\mathbf{r}) \sim \int f(\mathbf{r}, \mathbf{w}) \cdot (V_z(\mathbf{r}) - w_z)^2 d\mathbf{w}$$

and

$$T_\rho(\mathbf{r}) \sim \int f(\mathbf{r}, \mathbf{w}) \cdot (V_\rho(\mathbf{r}) - w_\rho)^2 d\mathbf{w}.$$

4. The correlation coefficient is given by:

$$K_{z\rho} \sim \int f(\mathbf{r}, \mathbf{w}) \cdot (V_z(\mathbf{r}) - w_z)(V_\rho(\mathbf{r}) - w_\rho) d\mathbf{w} \neq 0,$$

especially for the secondary interstellar atoms.

5. The third moment of $f(\mathbf{r}, \mathbf{w})$ for the secondary interstellar atoms is not zero:

$$K_{zzz} \sim \int f(\mathbf{r}, \mathbf{w}) \cdot (V_z(\mathbf{r}) - w_z)^3 d\mathbf{w} \neq 0.$$

This means that this distribution function is not symmetric relative to its maximum.

All these features are illustrated in Figs. 2.9 and 2.10. Figure 2.9 presents moments of $f(\mathbf{r}, \mathbf{w})$ at 90 AU as functions of angle θ . These results were obtained in the frame of the Baranov–Malama model with the following boundary conditions in the undisturbed LISM: the number densities of protons and neutral hydrogen atoms are $n_{p,\text{LISM}} = 0.06\text{cm}^{-3}$, $n_{\text{H,LISM}} = 0.18\text{cm}^{-3}$, respectively; the relative LISM/SW velocity is $V_{\text{LISM}} = 26.4\text{km/s}$, and the interstellar temperature is $T_{\text{LISM}} = 6519\text{K}$. For the inner boundary conditions at the Earth’s orbit the following parameters of the solar wind were adopted: $n_{p,E} = 6\text{cm}^{-3}$, $V_E = 441.9\text{km/s}$, and the Mach number $M_E = 4.034$. Note that in the 3D case, for example when the interstellar magnetic field is taken into account, the hydrogen distribution at 90 AU becomes asymmetric (due to three-dimensional structure of the heliospheric interface) and the non-Maxwellian properties are even more complex.

Note, also, that the previous attempt to treat the distribution function as non-Maxwellian has been done by Sherer et al. (1999). However, only the first and third properties listed above have been taken into account in their model, while Katushkina and Izmodenov (2010, 2011) studied all these non-Maxwellian features of the velocity distribution at 90 AU (that hereafter we call the global effects of the heliospheric interface). They concluded that these global effects are important and should be included in any theoretical model of H atoms distribution inside the heliosphere. Therefore, special boundary conditions for the velocity distribution function at 90 AU are necessary.

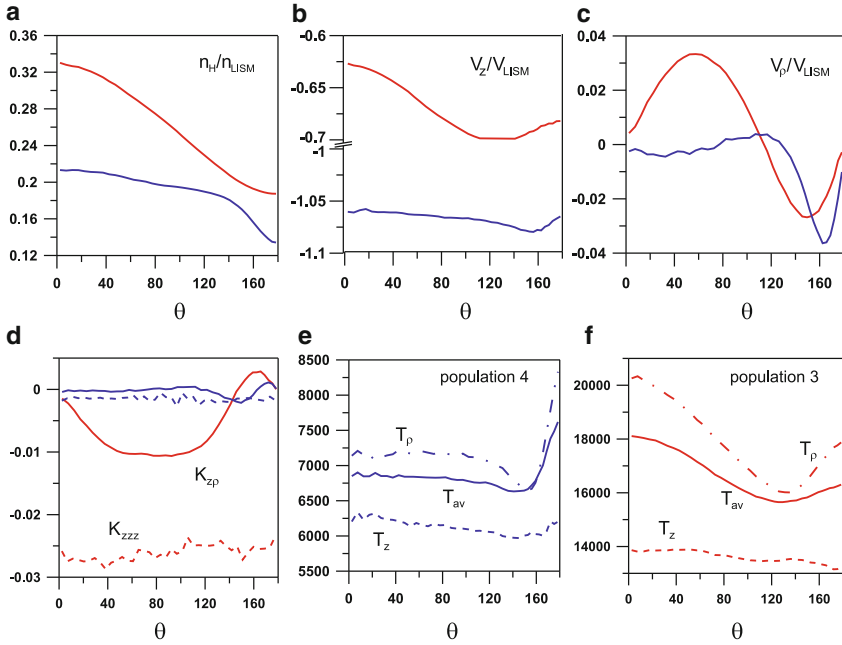


Figure 2.9: Number densities (a), bulk velocities (b, c), correlation coefficient $K_{z\rho}$ (d), third moment K_{zzz} , and kinetic “temperatures” T_z , T_ρ and T_{av} (e, f) of the primary (blue) and secondary (red) interstellar atoms at 90 AU as functions of angle θ from the upwind direction. $K_{z\rho}$ (d) and K_{zzz} are presented in dimensionless units; kinetic temperatures T_z , T_ρ and T_{av} are in Kelvins. T_{av} is an averaged temperature defined as $3 \cdot T_{av} = T_z + T_\rho + T_\varphi$.

Boundary Conditions

In this paper we consider three models of heliospheric H atoms. One of the three models (Model 3) includes the global effects mentioned above, while the two other models are more simplified. We will compare the results of the three models to identify and separate the effects of local and global phenomena on the distribution of H atoms in the heliosphere. The models differ only by the boundary conditions at 90 AU. A summary of the models discussed in this section is given in Table 2.2.

Model 1 is the one-component hot model that implies solution of the kinetic equation (2.4) with the Maxwellian velocity distribution function at the outer boundary. For the specific calculations performed in the frame of this model we use parameters of the Maxwellian distribution, i.e., the number density (n_H), bulk velocity ($V_{H,z}$), and temperature (T_H) calculated at 90 AU in the upwind direction in the frame of the Baranov–Malama model. These values at 90 AU are:

$$n_H = 0.54 \cdot n_{H,\text{LISM}}, \quad V_{H,z} = -0.79 \cdot V_{H,\text{LISM}}, \quad T_H = 15,000 \text{ K}.$$

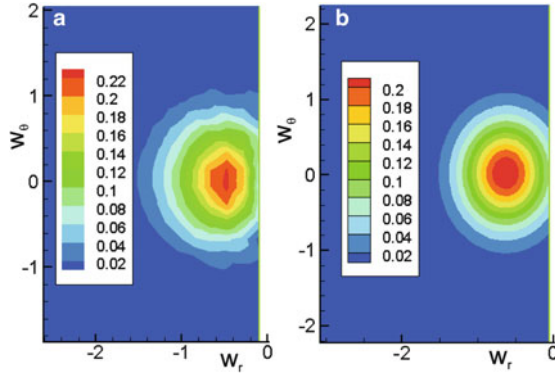


Figure 2.10: Illustration of the asymmetry of $f(\mathbf{r}, \mathbf{w})$ of the secondary interstellar atoms at 90 AU (for $\mathbf{w}_\varphi = 0$) in the upwind direction. Panel **a** presents the results of the Baranov–Malama model and shows an asymmetric $f(\mathbf{r}, \mathbf{w})$. For comparison, the symmetric velocity distribution calculated using Eq. (2.6) is shown in panel **b**. \mathbf{w}_r , \mathbf{w}_θ , \mathbf{w}_φ are velocity components in the spherical coordinate system

Table 2.2: Summary of the heliospheric models discussed in this manuscript

Model number	Model description
1	One-component hot model
2	Two-component hot model (Bzowski et al. 2008)
2b	Two-component hot model without ionization
3	Advanced model (Katushkina and Izmodenov 2011)
3b	Advanced model without ionization
3c	Advanced model without ionization plus flat solar Lyman- α spectrum

where $n_{\text{H,LISM}} = 0.18 \text{ cm}^{-3}$, $V_{\text{H,LISM}} = 26.4 \text{ km/s}$. These parameters correspond to the mixture of the primary and secondary interstellar atoms. Note that the effects of the heliospheric interface are treated very simply, assuming the parameters of the Maxwellian distribution are different from the parameters in the LISM.

Model 2 is the so-called two-component hot model (Bzowski et al. 2008). In this model, the kinetic equation (2.4) is solved separately for the primary and secondary populations of interstellar atoms. The velocity distribution functions are assumed to be Maxwellian for each of the populations and the parameters of the distribution functions are calculated in the frame of the Baranov–Malama model. These parameters for the primary interstellar atoms are:

$$n_{\text{H,prim}} = 0.22 \cdot n_{\text{H,LISM}}, \quad V_{z,\text{prim}} = -1.06 \cdot V_{\text{H,LISM}}, \quad T_{\text{H,prim}} = 6,840 \text{ K}.$$

The values for the secondary interstellar atoms are:

$$n_{\text{H,second}} = 0.32 \cdot n_{\text{H,LISM}}, \quad V_{z,\text{second}} = -0.63 \cdot V_{\text{H,LISM}}, \quad T_{\text{H,second}} = 18,126 \text{ K}.$$

As shown by [Katushkina and Izmodenov \(2010\)](#), model 2 leads to significant discrepancies in the distribution of H atoms inside the heliosphere as compared with the self-consistent Baranov–Malama model. This fact is related to the non-Maxwellian behavior of the velocity distribution function of hydrogen atoms inside the heliospheric interface ([Izmodenov et al. 2001](#); [Izmodenov 2001](#)).

In model 3, we use the boundary conditions that take into account all of the previously-mentioned kinetic effects at the outer boundary. This model will be called the advanced model of hydrogen distribution inside the heliosphere. Comparison of this model results with the Baranov–Malama model gives very good agreement ([Katushkina and Izmodenov 2011](#)) which confirms that all of the required kinetic effects are correctly implemented.

For the primary interstellar atoms, the distribution function at 90 AU is chosen as the 3D normal distribution:

$$\begin{aligned}
 f_s(\mathbf{r}, \mathbf{w}) = & \frac{n_H}{(2\pi)^{3/2} \cdot \sqrt{(D_\rho D_z - V_{z\rho}^2) D_\varphi}} \cdot \exp\left(-\frac{1}{2} \left(\frac{D_z}{D_\rho D_z - V_{z\rho}^2} (V_\rho - w_\rho)^2 \right. \right. \\
 & + \frac{1}{D_\varphi} (V_\varphi - w_\varphi)^2 + \frac{D_\rho}{D_\rho D_z - V_{z\rho}^2} (V_z - w_z)^2 \\
 & \left. \left. - 2 \cdot \frac{V_{z\rho}}{D_\rho D_z - V_{z\rho}^2} (V_\rho - w_\rho)(V_z - w_z) \right) \right) \quad (2.6)
 \end{aligned}$$

Here $D_R = \frac{k}{m_H} T_R$, $D_\varphi = \frac{k}{m_H} T_\varphi$, and $D_z = \frac{k}{m_H} T_z$. k is the Boltzmann constant and m_H is the mass of hydrogen atom. In this case all zeroth, first, and second moments of the velocity distribution function are taken into account and calculated in the frame of the Baranov–Malama model. However, for the population of the secondary interstellar atoms such an approach does not give a complete agreement with the Baranov–Malama model ([Katushkina and Izmodenov 2010](#)) because the distribution function of this population is asymmetric with respect to its maximum and has nonzero third moments, which are neglected in the 3D normal distribution (see Fig. 2.10). That is why for the secondary interstellar atoms [Katushkina and Izmodenov \(2011\)](#) used the velocity distribution function at 90 AU calculated using a Monte–Carlo scheme in the frame of the Baranov–Malama model. It was shown that 15–20 millions of unsplittable trajectories ([Malama 1991](#)) in the Monte–Carlo code is enough in order to get acceptable accuracy of calculations. Therefore, in this paper we will follow the [Katushkina and Izmodenov \(2010\)](#) approach, a 3D normal distribution for the primary interstellar atoms and use the numerically calculated velocity distribution function as the boundary conditions at 90 AU for the secondary interstellar atoms.

Calculations of hydrogen distribution inside the heliosphere by means of our advanced model consist of two separate steps. In the first step, a global heliospheric interface model (the Baranov–Malama model or its modern versions, for example [Malama et al. 2006](#); [Izmodenov et al. 2005](#)) is employed, and the hydrogen velocity distribution function and its moments at the boundary of 90 AU are obtained. In the second step we numerically solve the kinetic equation (2.4) with the boundary conditions obtained in the first step.

Among other advantages, this two-step procedure allows us to separate global effects of the heliospheric interface, which are taken into account in the first step,

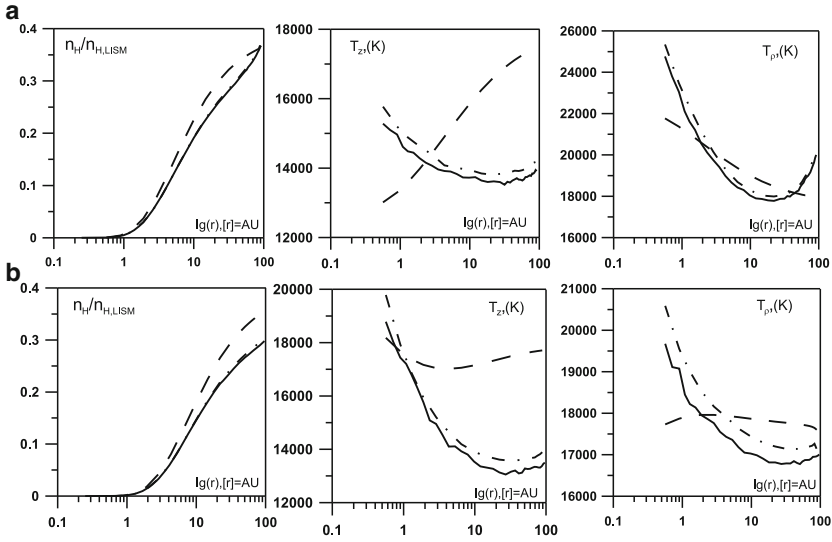


Figure 2.11: Parameters of the secondary interstellar atoms inside the heliosphere as functions of heliocentric distance along the upwind direction (a) and crosswind direction (b). *Solid curves* correspond to the results of the Baranov–Malama model; *dashed curves* correspond to the results of model 2; *dashed-dot curves* correspond to the advanced model 3. In these calculations $\mu = 1.258$, $\beta_{ph,E} = 1.16 \times 10^{-7} \text{ s}^{-1}$, $\beta_{ex,E} = 4.8 \times 10^{-7} \text{ s}^{-1}$. To calculate the charge-exchange rate at the Earth orbit, we applied averaged values of the solar wind number density (6 cm^{-3}) and velocity (440 km/s) known from measurements and the charge-exchange cross-section from Lindsay and Stebbing (2005) [From Katushkina and Izmodenov (2011)]

from local effects (i.e. within the heliosphere), which can be explored in the second step in details. These local effects may include time-dependent and 3D phenomena as described in the next section.

At the end of this section we illustrate the importance of the non-Maxwellian features at the outer boundary by comparing the results of model 2 and model 3 shown in Fig. 2.11. The results of the Baranov–Malama model are shown to verify precision of model 3.

Figure 2.11 presents the number density and effective kinetic “temperatures” of the gas along the upwind and crosswind directions. It is seen that there is a very good agreement between the results of the Baranov–Malama model and the advanced model of hydrogen distribution within 90 AU, while the two-component hot model leads to significant discrepancies. Firstly, the two-component hot model overestimates the number density of hydrogen everywhere in the heliosphere. This is because the two-component hot model assumes constant parameters of hydrogen at 90 AU, but due to the heliospheric interface effects the hydrogen parameters depend on angle θ (e.g. the number density at 90 AU decreases with θ). Second,

there are qualitative differences in the behavior of temperatures T_z in upwind and T_ρ in crosswind between model 2 and model 3. These differences are caused by the kinetic non-Maxwellian properties of the hydrogen distribution function at 90 AU which were described above.

Concluding this section we summarize that: 1. Kinetic features in the velocity distribution of H atoms in the outer heliosphere must be taken into account in theoretical models of hydrogen distribution inside the heliosphere. 2. A good agreement between the results of Baranov–Malama model and our advance model (model 3) implies that all important kinetic effects are included in the advanced hot model through the correctly chosen boundary conditions.

Modeling of Time-Dependent and Heliolatitudinal Effects

Both observations of the solar wind (McComas et al. 2008) and backscattered solar Lyman- α radiation (Bzowski et al. 2003; Quémerais et al. 2008; Lallement et al. 2010) have shown that the solar wind parameters vary with the solar cycle and have a three-dimensional (3D) nature, i.e. they depend on heliolatitude. Since the charge exchange ionization rate depends on the solar wind flux, then the 3D and time-dependent effects may change the distribution of the H atoms in the heliosphere (Bzowski 2003). In turn, the 3D and time-dependent nature of the H atom distribution may effect the maps of backscattered Lyman- α radiation. In this section we will describe the parameters and results of the 3D time-dependent model of the H atom distribution in the heliosphere.

To calculate the velocity and spatial distribution of H atoms in the heliosphere we employed the 3D time-dependent version of our advanced model (model 3) with the boundary conditions specified above. To finalize the formulation of the model we need to specify the photoionization rate $\beta_{ph,E}(t, \lambda)$, charge-exchange rate $\beta_{ex,E}(t, \lambda)$ and balanced parameter $\mu(t, \lambda, w_r)$ as functions of time, and heliolatitude λ . The parameter μ is also a function of radial component of atom velocity w_r because the flux of photons illuminating (and forcing) an atom depends on the atom’s velocity. Here we follow the approach used by Bzowski et al. (2013, this volume).

To calculate the photoionization rate as a function of time in the ecliptic plane we use the SOLAR2000 database (<http://www.spacewx.com/solar2000.html>; the Solar Irradiance Platform (SIP), formerly known as the SOLAR2000 irradiance specification tool, produces the variable, full solar spectrum in assorted spectral formats for historical, nowcast, and forecast applications). The time resolution is one day. In the calculations we neglect the angle between the solar equatorial and ecliptic planes, i.e. we assume that from SOLAR2000 we get $\beta_{ph,E}(t, \lambda = 0)$. Magnitudes of $\beta_{ph,E}(t, \lambda = 0)$ were adjusted from the Earth orbit to 1 AU and then averaged over one Carrington rotation.

To calculate the charge-exchange ionization rate in the ecliptic plane we use hourly data of the solar wind number density ($n_{p,E}(t)$) and velocity ($w_{sw,E}(t)$) from the OMNI database (<http://omniweb.gsfc.nasa.gov/>; the OMNIWeb interface provides access to the multi-source OMNI 2 dataset; the OMNI 2 dataset contains hourly resolution solar wind magnetic field and plasma data from many spacecraft in geocentric orbit and in orbit about the L1 Lagrange point). These hourly data

were used to calculate fluxes of mass, momentum and energy. The fluxes with hourly resolution were used to calculate the averaged fluxes (over one day), which were adjusted to 1 AU from the Earth orbit. Then these data were averaged over one Carrington rotation. The charge-exchange ionization rate can be calculated as follows:

$$\beta_{ex,E}(t, 0) = n_{p,E}(t) \cdot w_{sw,E}(t) \cdot \sigma(w_{sw,E}),$$

where $\sigma(w_{sw,E})$ is the charge-exchange cross-section (Lindsay and Stebbing 2005). The total ionization rate for $\lambda = 0$ is calculated as

$$\beta_{tot,E}(t, \lambda = 0) = \beta_{ex,E}(t, 0) + \beta_{ph,E}(t, 0).$$

The heliolatitudinal dependence for the total ionization rate $\beta_{tot,E}(t, \lambda)$ has been calculated using SOHO/SWAN data. A detailed description of how to get the total ionization rate $\beta_{tot,SWAN}(t, \lambda)$ from SOHO/SWAN is given in Qu  merais et al. (2006). Overall, $\beta_{tot,E}(t, \lambda)$ is determined as follows:

$$\beta_{tot,E}(t, \lambda) = \beta_{tot,E}(t, 0) \cdot \frac{\beta_{tot,SWAN}(t, \lambda)}{\beta_{tot,SWAN}(t, 0)}.$$

Since the time-resolution of $\beta_{tot,SWAN}(t, \lambda)$ is sometime smaller than 27 days to get the value at a given day we make a linear interpolation.

To calculate the parameter μ_{eq} in the solar equator plane ($\lambda = 0$) as a function of time (for $w_r = 0$) we use solar Lyman- α flux from the LASP Interactive Solar Irradiance Data center (<http://lasp.colorado.edu/lisird/lya/>). From this database we get the solar Lyman- α flux as a function of time with a resolution of one day. Then these data are adjusted to 1 AU from the Earth orbit and averaged over one Carrington rotation. We assumed that $\mu_{eq}(t, w_r = 0) = 0.9 \cdot F_{solar}(t)/F_{solar,0}$, where $F_{solar,0} = 3.32 \cdot 10^{11} \text{ ph}/(\text{s}/\text{cm}^2 \cdot \text{\AA})$ is the total Lyman- α flux at the line center. For the dependence of μ on the radial component of velocity an analytical formula obtained by Bzowski (2008) was employed, namely:

$$\mu_{eq}(t, w_r) = \mu_{eq}(t, w_r = 0) \cdot \frac{F_B(F_{solar}(t), w_r)}{F_B(F_{solar}(t), w_r = 0)},$$

where F_B is a function described in Bzowski (2008).

To get the heliolatitudinal dependence of μ we use the following expression from Pryor et al. (1992):

$$\mu(t, \lambda, w_r) = \mu_{pole}(t, w_r) + \cos^2(\lambda) \cdot (\mu_{eq}(t, w_r) - \mu_{pole}(t, w_r)),$$

where

$$\mu_{pole}(t, w_r) = F_B(F_{solar} - \Delta F_{solar}, w_r)$$

and $\Delta F_{solar} \approx 0.05 \cdot 10^{11} \text{ ph}/(\text{cm}^2\text{s})$, this value is given from Pryor et al. (1998). The resulting functions of $\beta_{tot,E}$, $\beta_{ex,E}$, $\beta_{ph,E}$, and μ are shown in Figs. 2.12, 2.13 and 2.14.

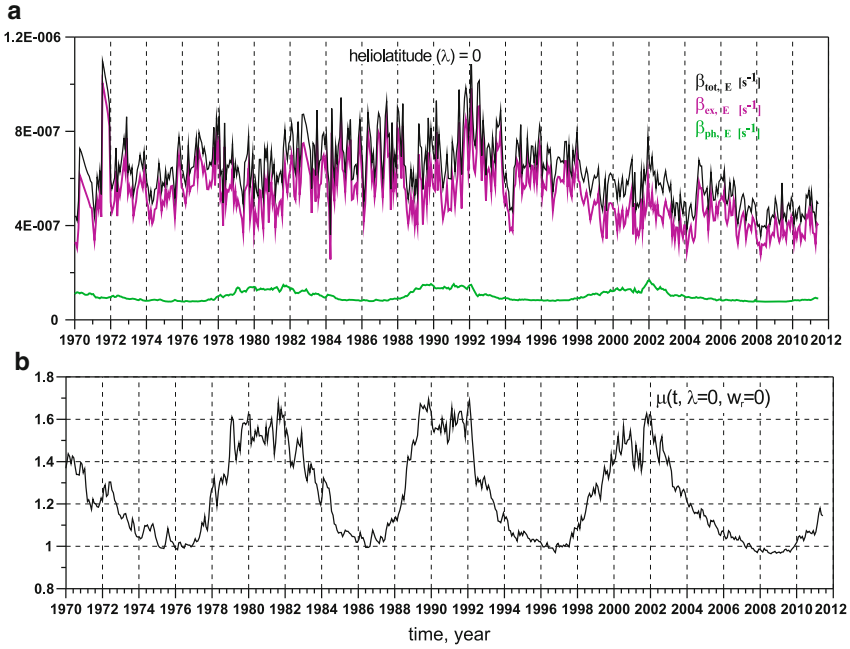


Figure 2.12: (a) Time dependence of the total ionization rate ($\beta_{\text{tot},E}$), charge-exchange rate ($\beta_{\text{ex},E}$) and photoionization rate ($\beta_{\text{ph},E}$) at the Earth's orbit in the solar equatorial plane ($\lambda = 0$). (b) Time dependence of the radiation pressure parameter μ for $\lambda = 0$ and $w_r = 0$

Results of the Advanced Hot Model in the 3D Non-Stationary Case

Figures 2.15 and 2.16 show the number densities, radial components of the bulk velocities V_r , and the radial kinetic temperatures T_r for the primary and secondary interstellar atoms in the upwind direction as functions of time. The distributions are shown for different heliocentric distances. As shown in the figures, the time-variations of the number densities of the primary and secondary populations behave qualitatively the same and both are anti-correlated with the time variations of the ionization rate. For example, in 2002 at solar maximum there is a maximum of ionization rate as shown in Fig. 2.12a and a minimum of the H atom number densities. Note that charge exchange provides the main contribution to the total ionization rate since the charge exchange rate exceeds the photoionization rate significantly. The local maximum of the number densities in 2004–2005 is due to the local minimum of the charge exchange rate. There is a monotonic decrease of the solar activity and therefore ionization rate from 2005 to 2008 that results in a continuous increase of the number density from 2005 to 2008. There is an abrupt fall number density in 2009 caused by the increase in the charge exchange rate.

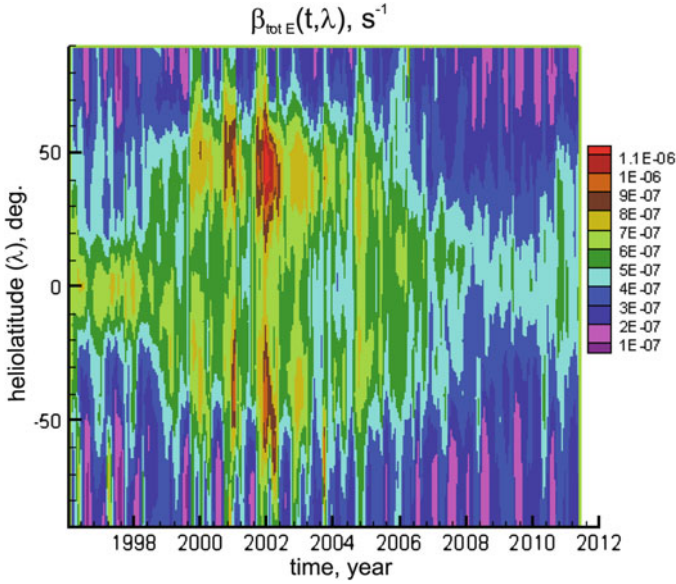


Figure 2.13: Total ionization rate as a function on time and heliolatitude

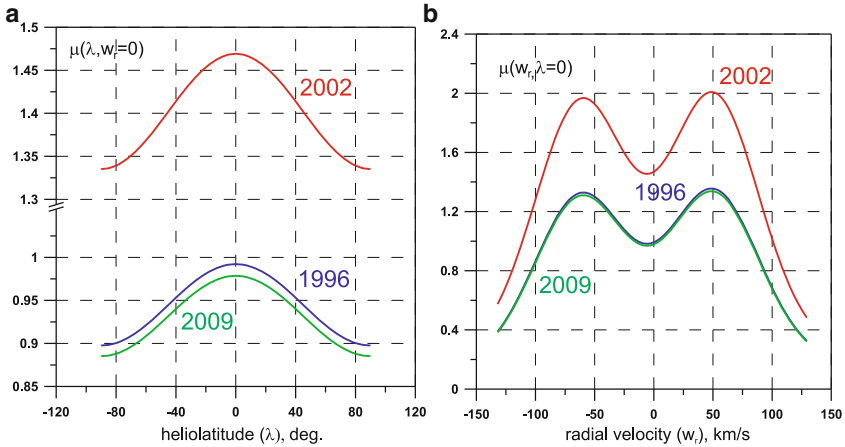


Figure 2.14: (a) Parameter μ as a function of heliolatitude λ for $w_r = 0$; (b) μ as a function of radial velocity w_r for $\lambda = 0$. Red curves correspond to solar maximum conditions (2002), blue curves correspond to solar minimum conditions (1996), green curves correspond to the 2009 solar minimum

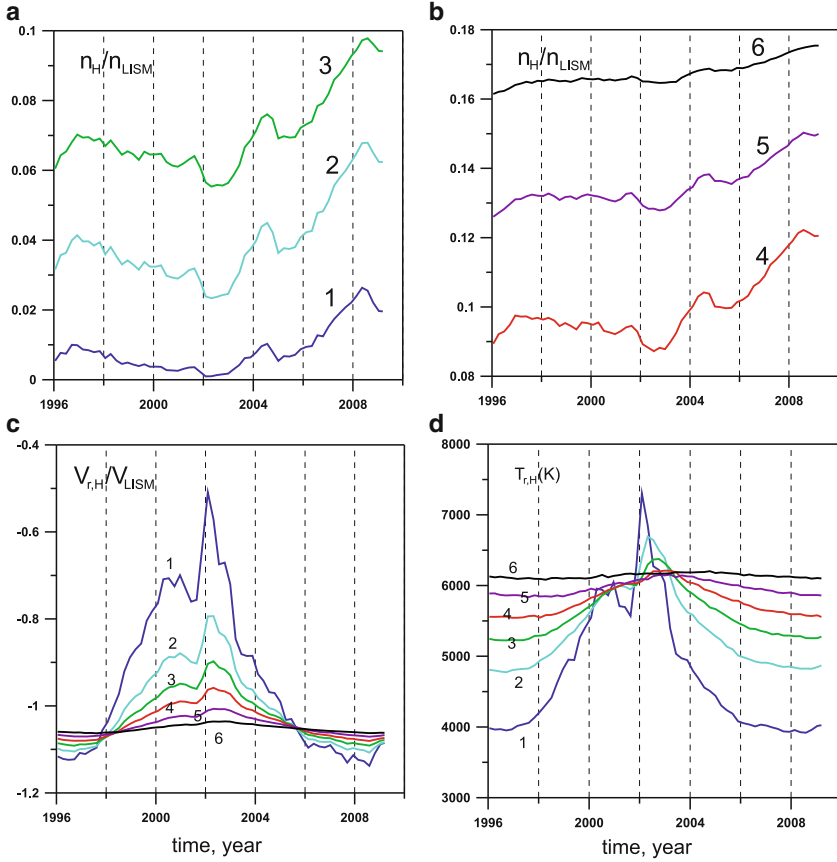


Figure 2.15: Distribution of the number density (a, b), radial velocity (c) and radial kinetic temperature (d) of the **primary interstellar atoms** along the upwind direction as functions of time; different colors correspond to different heliocentric distances: (1) $r = 1$ AU, (2) $r = 2$ AU (3) $r = 3$ AU, (4) $r = 4.4$ AU, (5) $r = 7.4$ AU, (6) $r = 10$ AU

It can be seen from the figures that time fluctuations of all parameters are small at 10 AU and beyond. Therefore, local effects become small for $r > 10$ AU in the upwind direction, in agreement with [Ruciński and Bzowski \(1995\)](#).

Let us focus on the bulk velocities of the H atoms in the upwind direction. Figures 2.15c and 2.16c show that the time-variation of the bulk velocities is very similar to the time variation of $\mu(t)$, shown in Fig. 2.12b. Therefore, fluctuations of the bulk velocities of the primary and secondary atoms are mainly determined by the force changing the atom trajectories rather than the ionization processes.

However, a qualitative difference in the behavior of the primary and secondary H atoms appears when the heliocentric distance increases. In Fig. 2.15c for the primary population all curves cross each other at two time periods in 1998 and

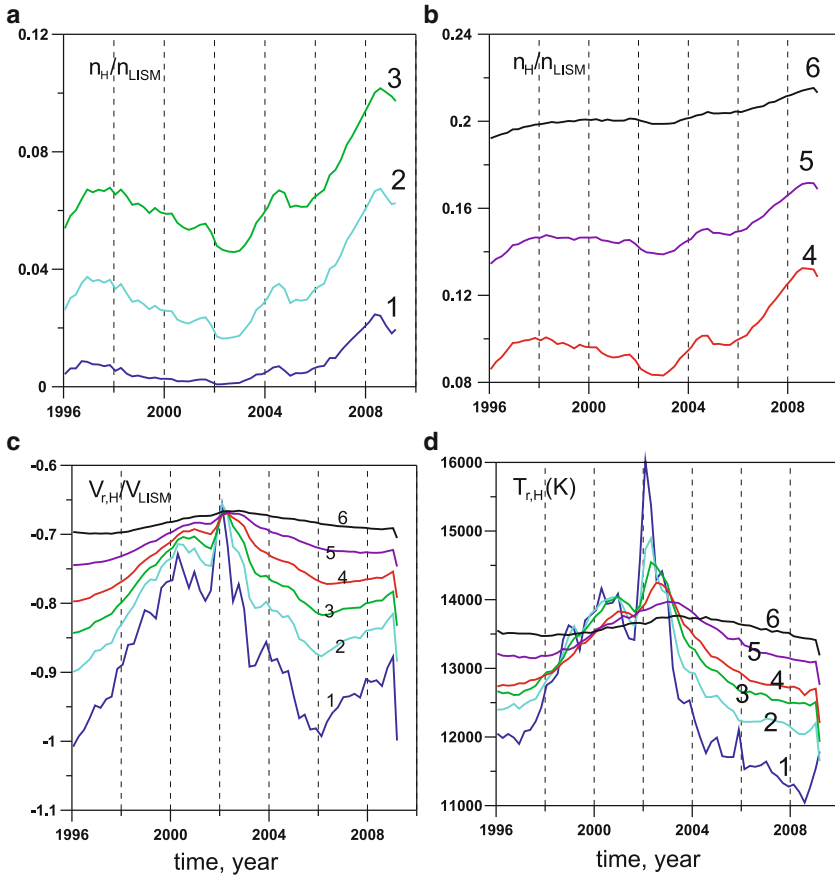


Figure 2.16: Distribution of the number density (a, b), radial velocity (c) and radial kinetic temperature (d) of the **secondary interstellar atoms** along the upwind kinetic direction as functions of time; different colors correspond to different heliocentric distances: (1) $r = 1$ AU, (2) $r = 2$ AU (3) $r = 3$ AU, (4) $r = 4.4$ AU, (5) $r = 7.4$ AU, (6) $r = 10$ AU

2006. Approximately in these periods of time $\mu(t, \lambda = 0, w_r = 0) \approx 1$ in the ecliptic plane, i.e. solar radiation pressure balances solar gravitation, and the trajectories of the atoms are straight lines. In this situation the bulk velocity of the gas would be constant if the ionization processes were absent. However, due to the so-called selection effect, the bulk velocity of the atoms would increase toward the Sun. The selection effect is connected with the fact that the slow atoms have more chances to be ionized before they reach the same heliocentric distance as the fast atoms. It is simply because the slow atoms spend more time along their trajectory. As a result of the selection, the maximum of the velocity distribution function of H

atoms moves towards larger velocities, and the bulk velocity increases. This effect was discussed in [Lallement et al. \(1985a\)](#) and [Bzowski et al. \(1997\)](#).

When $\mu > 1$, the effective force decelerates the atoms as they approach the Sun. For $\mu \approx 1.1$, the effect of the deceleration due to the effective force compensates the selection effect. In this case the bulk velocity practically does not change when the atoms approach the Sun. In the case of $\mu > 1.1$, as it was from 1998 to 2006, the repulsive force decelerates the atoms and the bulk velocity of the gas becomes smaller. The smallest bulk velocity was in 2002 when the repulsive force had its maximum. Also, for $\mu > 1.1$ and some fixed moment of time, the bulk velocity decreases towards the Sun. In the case of $\mu < 1$ the bulk velocity increases towards the Sun.

For the secondary interstellar atoms the situation is slightly different. This population is slower than the primary population, and approaching the Sun the atoms are more effectively ionized. As a result, the bulk velocity of the secondary interstellar atoms increases towards the Sun during the entire period considered with the exception of the 2002 solar maximum when the bulk velocity did not change with heliocentric distance.

Another qualitative difference between the primary and secondary populations is in the behavior of the bulk velocity in the period from 2006 to 2009. As it was mentioned before, the behavior of the bulk velocity for the primary populations reflects time-variations of $\mu(t)$, while for the secondary population the bulk velocity decreases from 2006 to 2008 and then rapidly increases in 2009. Such a behavior of the bulk velocity can be explained by the strong decrease in the charge-exchange rate before 2008. A strong increase of the bulk velocity in 2009 is due to the increase in the charge exchange rate in 2009 and the corresponding increase of the selection effect.

Now, let us focus on the kinetic temperature T_r , that is the second moment of the velocity distribution function calculated for radial velocity component. Figures 2.15d and 2.16d show that the temperatures of the primary and secondary populations are qualitatively similar in behavior. For a small heliocentric distance the time variations of T_r resembles $\mu(t)$. This means the radial temperature (as well as the bulk velocity) is mainly affected by the resulting force. However, the ionization processes are important as well. For example, the temperature decreases towards the Sun for both the primary and secondary populations except near solar maximum. Figure 2.17 presents the number density of both populations of interstellar hydrogen as functions of time and heliocentric distance along the upwind direction.

Figure 2.18 shows sky-maps of the number densities, radial velocities and kinetic temperature T_r of the primary and secondary interstellar atoms at 1 AU calculated for 1996, i.e. for the minimum of solar activity. The upwind direction has the following heliographic coordinates: heliolongitude $\alpha_{HGI} = 178.98^\circ \pm 0.5^\circ$ and heliolatitude $\beta_{HGI} = 5.11^\circ \pm 0.2^\circ$. It is seen (Fig. 2.18a, d) that the maxima of the H atom number densities occur at the upwind heliolongitude. For this upwind heliolongitude there are two maxima in the southern and northern hemispheres and a minimum in the plane of the solar equator. This minimum in number density is due to the maximum of the ionization rate near the solar equatorial plane. The distributions of radial velocity, Fig. 2.18b, e, show minima near the upwind direc-

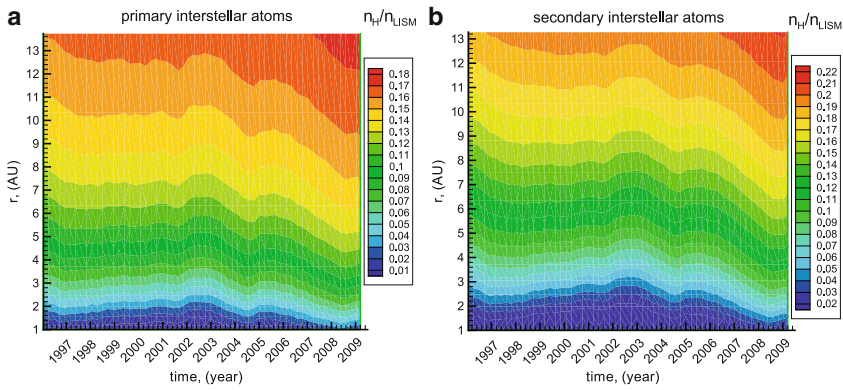


Figure 2.17: Number density of the primary and secondary interstellar atoms in the upwind direction as functions of time and heliocentric distance

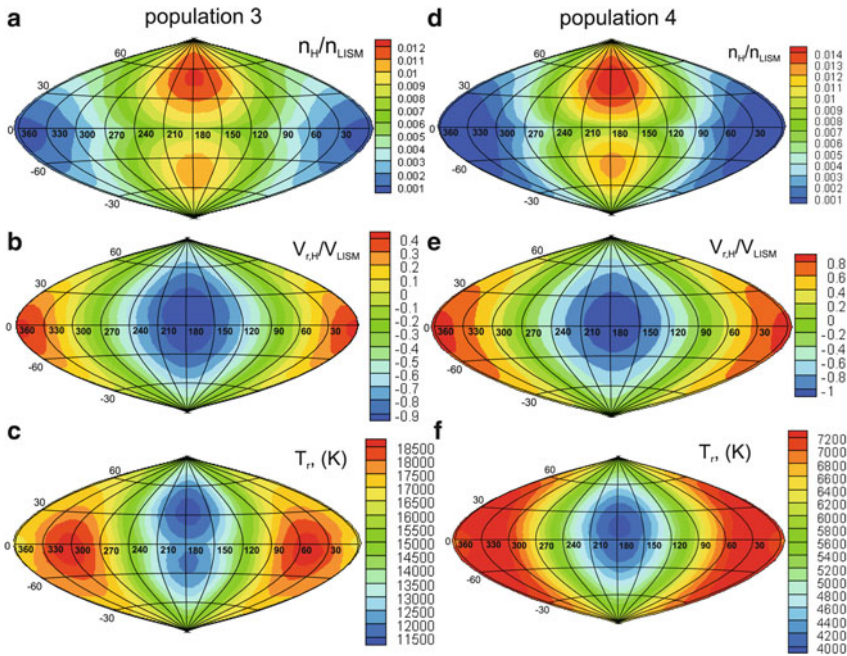


Figure 2.18: Number density (a, d), radial velocity (b, e) and radial kinetic temperature (c, f) of the secondary (population 3, left column) and primary (population 4, right column) interstellar atoms, calculated at 1 AU as functions of heliolatitude and heliolongitude in the heliographic coordinate system (HGI). These results are obtained for solar minimum conditions (year 1996), when the heliolatitudinal dependence of the total ionization rate is very strong. In HGI coordinates, the upwind direction is at 178.98° in heliolongitude and at 5.11° of heliolatitude

tion. Similar minima in the upwind direction are seen in the maps of the radial kinetic temperature T_r (Fig. 2.18c, f). However, the temperature maps also show heliolatitudinal effects. The latitudinal effect is more pronounced for the secondary population.

Application of the Hydrogen Distribution Models for Calculation of the Backscattered Solar Lyman- α

In this section we will demonstrate how the model described above can be applied to the analyzes of the backscattered solar Lyman- α and also, in the simplest case, how the effects of the heliospheric interface are pronounced in the intensities, line-shifts, and line-widths of the heliospheric Lyman- α radiation.

Modeling Backscattered Solar Lyman- α Profiles

The profiles of backscattered Lyman- α radiation $I(\mathbf{r}, \nu, \boldsymbol{\Omega})$ were computed for anti-solar radial directions ($\boldsymbol{\Omega}$) for an observer located at 1 AU. Here \mathbf{r} is a position of the observer, ν is the frequency of the backscattered radiation, $\boldsymbol{\Omega}$ is the line-of-sight direction. We use the “self-absorption” approximation (Quémerais 2000). In this approximation only singly scattered photons are considered (i.e. multiply scattered photons are neglected), and the absorption of photons between the Sun and the scattering point is neglected. As was shown in Quémerais and Izmodenov (2002), the simplified “self-absorption” approach gives similar results as compared with a full radiative transfer model. For the line-width of the backscattered profile at 1 AU the difference between the full radiative transfer model and the self-absorption model is less than 15 % for the upwind direction and becomes smaller as the line-of-sight moves from upwind to downwind. In the downwind direction two approaches give nearly the same line-widths. The simplified self-absorption approach is sufficient for the purposes of this paper. As will be shown below, the effects of the heliospheric interface are larger than the difference between the full radiative transfer and self-absorption models.

The radiative transfer equation for $I(\mathbf{r}, \nu, \boldsymbol{\Omega})$ can be written as follows:

$$\boldsymbol{\Omega} \cdot \nabla I(\mathbf{r}, \nu, \boldsymbol{\Omega}) = -\sigma_\nu(\mathbf{r}, \nu) n_H(\mathbf{r}) I(\mathbf{r}, \nu, \boldsymbol{\Omega}) + n_H(\mathbf{r}) j(\mathbf{r}, \nu, -\boldsymbol{\Omega}). \quad (2.7)$$

Here $n_H(\mathbf{r})$ is the number density of hydrogen atoms, $\sigma_\nu(\mathbf{r}, \nu)$ is the differential scattering cross-section that is proportional to the projection of the hydrogen distribution function on the line-of-sight, $j(\mathbf{r}, \nu, -\boldsymbol{\Omega})$ is the atomic emission coefficient which measures the number of photons emitted by a hydrogen atom per second per frequency unit and per solid angle. Note that scattered photons travel in the direction opposite to the line-of-sight direction, i.e. in $-\boldsymbol{\Omega}$. The first term on the right hand side of Eq. (2.7) is the loss term due to absorption of the scattered photons. The second term is the local source of emission due to the scattering process.

Equation (2.7) has the following solution in the self-absorption approximation:

$$I(\mathbf{r}, \nu, \boldsymbol{\Omega}) = \frac{4\pi}{10^6} \int_0^\infty n_H(\mathbf{r} + s\boldsymbol{\Omega}) j(\mathbf{r} + s\boldsymbol{\Omega}, \nu, -\boldsymbol{\Omega}) e^{-\tau_\nu(\mathbf{r} + s\boldsymbol{\Omega}, \mathbf{r})} ds, \quad (2.8)$$

where s is the coordinate along the line-of-sight, $\tau_\nu(\mathbf{r}', \mathbf{r})$ is the optical thickness for scattered photons with the frequency ν calculated from the scattered point $\mathbf{r}' = \mathbf{r} + s\boldsymbol{\Omega}$ for an observer located at point \mathbf{r} . The atomic emission coefficient j can be represented by:

$$j(\mathbf{r}', \nu, -\boldsymbol{\Omega}) = \phi(\omega) F_S(\mathbf{r}', \nu_p) \sigma_\nu(\mathbf{r}', \nu). \quad (2.9)$$

Here $\phi(\omega)$ is the scattering phase function that gives the relation between the directions of propagation of the photon before and after the scattering (Brandt and Chamberlain 1959). $F_S(\mathbf{r}', \nu_p)$ is the flux of the solar Lyman- α photons with the frequency of ν_p at point \mathbf{r}' . The solar Lyman- α spectra obtained by Lemaire et al. (1998) is used to calculate the solar Lyman- α flux at the Earth orbit at a given frequency ν .

In the case when the line-of-sight is radial, there is a simple relation between the frequency of the primary solar photon ν_p and the frequency of the backscattered photon ν : $\nu_p = 2 \cdot \nu_0 - \nu$, ν_0 is the frequency at line center. Thus, if we know the hydrogen velocity distribution function in the entire heliosphere, we can calculate the profiles of the backscattered Lyman- α radiation.

Since we consider two different populations of the interstellar H atoms inside the heliosphere and neglect multiple scattering effects, it becomes possible to calculate profiles of the radiation scattered by each populations separately. To do this we consider photons that were scattered by the primary and secondary interstellar atoms independently. Optical thickness is calculated for the mixture of the primary and secondary atoms, because a photon scattered, for example, by the primary interstellar atom can then be absorbed by atoms of both populations.

We can calculate the following moments of the backscattered radiation profiles:

- (a) Intensity measured in [R],

$$I_{\text{los}}(\mathbf{r}, \boldsymbol{\Omega}) = \int_0^\infty I(\mathbf{r}, \nu, \boldsymbol{\Omega}) d\nu;$$

- (b) Line-shift, expressed in km/s,

$$V_{\text{los}}(\mathbf{r}, \boldsymbol{\Omega}) = \frac{\int_0^\infty u(\nu) I(\mathbf{r}, \nu, \boldsymbol{\Omega}) d\nu}{I_{\text{los}}(\mathbf{r}, \boldsymbol{\Omega})};$$

- (c) Line-width, expressed in degrees Kelvin,

$$T_{\text{los}}(\mathbf{r}, \boldsymbol{\Omega}) = \frac{m_H}{k_b} \frac{\int_0^\infty (u(\nu) - V_{\text{los}}(\mathbf{r}, \boldsymbol{\Omega}))^2 I(\mathbf{r}, \nu, \boldsymbol{\Omega}) d\nu}{I_{\text{los}}(\mathbf{r}, \boldsymbol{\Omega})}.$$

Here, $u(\nu) = c(\nu/\nu_0 - 1)$, m_H is the mass of a hydrogen atom, k_b is the Boltzmann constant. The line-shift of the spectra is often called the line-of sight velocity, and the line-width is called the line-of-sight (or apparent) temperature. These integral characteristics of the backscattered Lyman- α profile reflect the properties of the velocity distribution function of the H atoms inside the heliosphere, but they do not coincide and should not be confused with the bulk velocity and temperature of the gas far away from the Sun.

Model Results for the Two-Dimensional Stationary Case

We have computed the backscattered Lyman- α profiles and their moments using three models of the hydrogen distribution inside the heliosphere described above. All calculations were performed for the anti-solar directions. For the 2D axisymmetric problem considered here each line of sight is characterized by the angle θ that is measured from the z-axis as shown in Fig. 2.8.

Figure 2.19 shows the intensities (left column), line-shifts (center-column) and line-widths (right column) of the backscattered Lyman- α radiation at 1 AU as functions of the line-of-sight angle θ . For models 2 and 3 the profiles of the photons scattered by the primary and secondary interstellar H atoms were computed separately (plots b, c in Fig. 2.19). The total backscattered profile is shown in plot a of Fig. 2.19. For model 1, which has only one component of atomic hydrogen, we computed only the characteristics of the total Lyman- α radiation.

For the total radiation (row a of Fig. 2.19), models 1 and 2 lead to a systematic increase in the intensities as compared with the intensities calculated for model 3. Comparison of models 2 and 3 for the primary and secondary populations (plots b and c) shows that the increase in the intensities is due to the secondary H atom component (compare left-columns in the plots a and c). Models 2 and 3 agree nicely for the primary H atom component.

Now, we will explore the main reason for the different results obtained from models 2 and 3. The models differ only in the boundary condition. We can identify two differences. The first one is the dependence of the boundary conditions on the angle θ in model 3, which does not exist in model 2. The second difference is the non-Maxwellian velocity distribution function at 90 AU in model 3, while in model 2 the velocity distribution is Maxwellian. To explore which one of the two identified differences mainly affects the spectral properties of the Lyman- α radiation we performed an additional model calculation (model 2a). In model 2a we assume that the velocity distribution functions at the outer boundary are Maxwellian for both the primary and the secondary populations of the H atoms. However, the parameters of the Maxwellians (i.e. number density, bulk velocity and temperature) are functions of the angle θ and they were calculated in the frame of the Baranov–Malama model. Therefore, model 2a allows to separate the effects of non-uniform flow of H atoms at 90 AU from the kinetic effects related to the non-Maxwellian features of the velocity distribution function.

Intensities, line-shifts and line-widths calculated in the frame of model 2a are also shown in Fig. 2.19a. It is seen that model 2a and model 3 produce very close results in the backscattered Lyman- α intensities, although there is a difference of ~ 20 Rayleigh for the upwind direction. It means that the main difference between models 2 and 3 is due to the non-uniform flow of H atoms at 90 AU in model 3. However, there is still a small difference due to the non-Maxwellian behavior of the velocity distribution function at 90 AU (which is taken into account only in model 3).

At first sight, it is not evident why the angular dependence of the H atom parameters at 90 AU would strongly influence the backscattered Lyman- α emission measured at 1 AU. It is especially so, because the main emissivity region for the backscattered Lyman- α radiation at 1 AU is located approximately at 2 AU for the

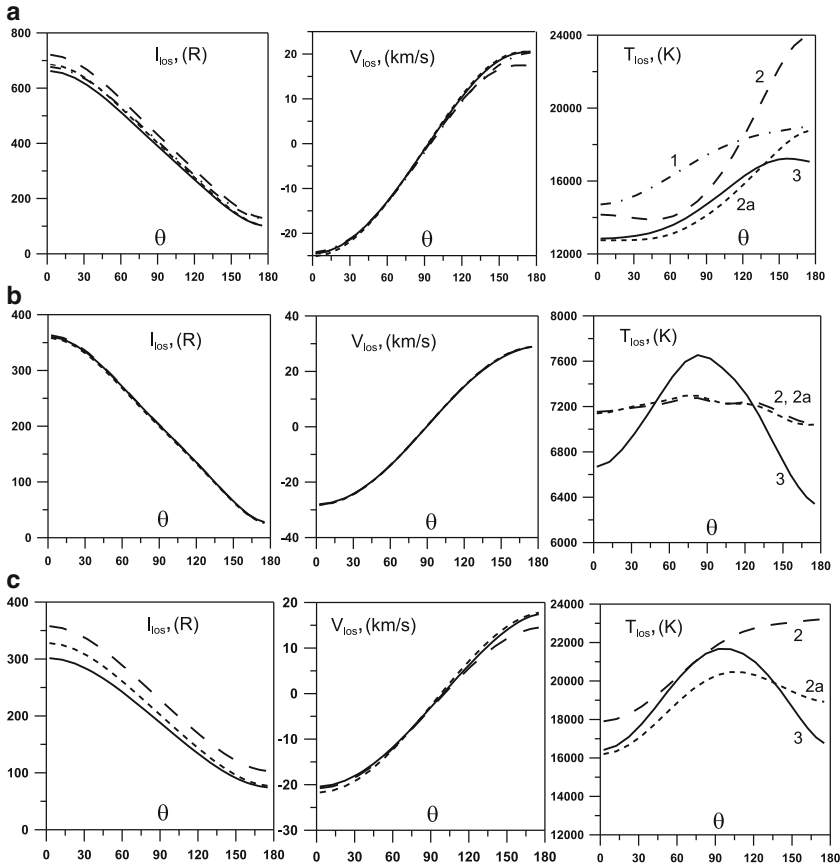


Figure 2.19: Intensities (*left column*), line-shifts (*center-column*) and line-widths (*right column*) of the backscattered Lyman- α radiation at 1 AU as functions of the line-of-sight angle θ from the upwind direction. Plots **a** (*top row*) are for the total radiation scattered by both primary and secondary interstellar atoms. Plots **b** (*middle row*) are for photons that were scattered by the primary interstellar atoms. Plots **c** (*bottom row*) correspond to the radiation scattered by the secondary interstellar atoms. Different curves correspond to three models of the hydrogen distributions in the heliosphere: (1) is the one-component hot model (model 1); (2) is the two-component hot model (model 2); (3) is our model (model 3) that takes into account effects of the heliospheric interface; additional curves marked as 2a in plots **a**, **b**, **c** correspond to the model of H atoms described in this section: model 2a which corresponds to model 2 plus the θ -dependence of hydrogen parameters at the outer boundary [From [Katushkina and Izmodenov \(2011\)](#)]

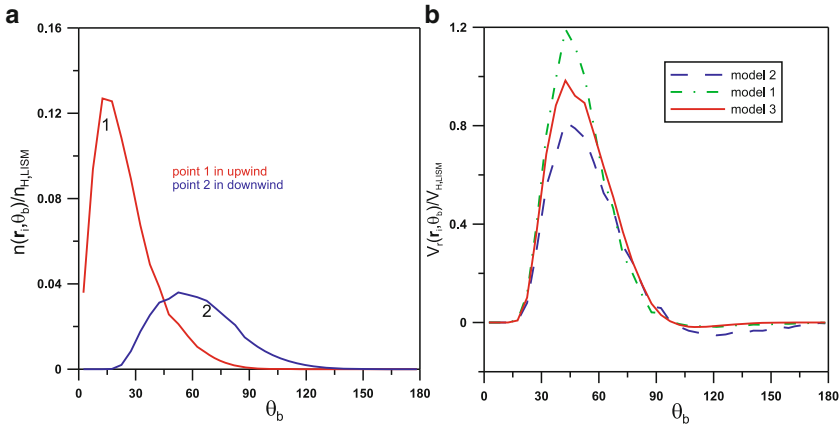


Figure 2.20: Contributions to the total number density (a) and radial velocity (b) of atoms arriving from various directions. Curve 1 in plot (a) corresponds to point 1 ($r_1 = 2$ AU, $\theta = 0^\circ$), and curve 2 corresponds to point 2 ($r_2 = 7$ AU, $\theta = 180^\circ$). The contribution to the radial velocity was calculated only for point 2. Various curves in plot (b) correspond to various models of hydrogen distribution: the *solid line* is model 3, the *dashed line* is model 2 and the *dashed-dot line* is model 1. All calculations are performed for a mixture of primary and secondary interstellar atoms [From [Katushkina and Izmodenov \(2011\)](#)]

upwind line-of-sight and at 7 AU for downwind. From the simple (naive) consideration one could expect that most of the H atoms in the regions close to the Sun would arrive from upwind. However, [Lallement and Bertaux \(1990\)](#) have shown (in the case of the hot model) that most of the atoms arrive into the vicinity of the Sun not exactly from upwind, since the thermal velocities of hydrogen atoms at the boundary are large enough compared to the bulk velocities. The same is true for our model. To illustrate this we calculate the function $n(\mathbf{r}_i, \theta_b)$ for two points ($i = 1, 2$) which correspond to the maximum emissivity region. Point 1 is located in the upwind direction at 2 AU from the Sun; point 2 is located in the downwind direction at 7 AU from the Sun. The function $n(\mathbf{r}_i, \theta_b)$ represents the contribution to the total number density at a given point (point 1 for curve 1 in Fig. 2.20a and point 2 for curve 2) from these particles which cross the outer boundary of 90 AU at $\theta = \theta_b$. This function $n(\mathbf{r}_i, \theta_b)$ is defined as follows:

$$n(\mathbf{r}_1, \theta_b) = \int_{\Omega_1} f(\mathbf{r}_1, \mathbf{w}_1) d\mathbf{w}_1. \quad (2.10)$$

Here f is the velocity distribution function of H atoms. The integration is performed over those \mathbf{w}_1 that correspond to the trajectories crossing the outer sphere of 90 AU at $\theta = \theta_b$. Here for simplicity we assume a balance between the solar gravitation and radiation pressure (i.e. $\mu = 1$). This means that all atomic trajectories are straight lines. In that case, the subspace Ω_1 is a cone with an apex angle

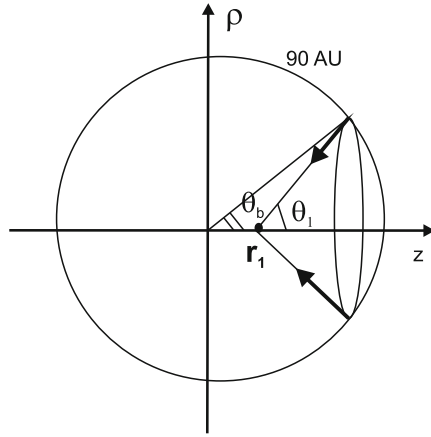


Figure 2.21: Schematic picture of penetration of the hydrogen atoms from the outer boundary to the vicinity of the Sun. Point 1 (\mathbf{r}_1) is located in the upwind direction at 2 AU from the Sun. In the case of straight atom's trajectories we consider only those atoms that arrive to point 1 from the outer boundary at θ_b . The angle θ_1 can be determined if we know r_1 and θ_b [From [Katushkina and Izmodenov \(2011\)](#)]

equal to θ_1 , as can be seen from Fig. 2.21. Let us introduce a spherical coordinate system in velocity space. It means that we describe the velocity vector \mathbf{w} by its modulus \tilde{w} and two spherical angles $\tilde{\theta}$ and $\tilde{\varphi}$, i.e. orthogonal coordinates of vector \mathbf{w} can be represented as follows:

$$\begin{aligned} w_x &= \tilde{w} \cdot \sin(\tilde{\theta}) \cdot \cos(\tilde{\varphi}) \\ w_y &= \tilde{w} \cdot \sin(\tilde{\theta}) \cdot \sin(\tilde{\varphi}) \\ w_z &= -\tilde{w} \cdot \cos(\tilde{\theta}) \end{aligned}$$

In spherical coordinates, $d\mathbf{w}_1 = \tilde{w}_1^2 \sin(\tilde{\theta}) d\tilde{w}_1 d\tilde{\theta} d\tilde{\varphi}$. For velocities from the subspace Ω_1 , $\tilde{\theta} = \theta_1 = \text{const}$ for the chosen value of θ_b and integration over $\tilde{\theta}$ is not needed. Hence, for our case Eq. (2.10) can be rewritten in the following form:

$$n(\mathbf{r}_1, \theta_b) = \int_0^{+\infty} \int_0^{2\pi} f(\mathbf{r}_1, \tilde{w}_1, \tilde{\theta} = \theta_1, \tilde{\varphi}) \tilde{w}_1^2 \sin(\theta_1) d\tilde{w}_1 d\tilde{\varphi}. \quad (2.11)$$

Now, in the case of $\mu = 1$:

$$f(\mathbf{r}_1, \tilde{w}_1, \theta_1, \tilde{\varphi}) = f_b(\theta_b, \tilde{w}_1, \theta_1, \tilde{\varphi}) \cdot \exp(-A(\mathbf{r}_1, \theta_b, \tilde{w}_1)),$$

where f_b is the corresponding velocity distribution function at 90 AU, A is the loss of hydrogen atoms along its trajectory from the outer boundary to point 1 due to the ionization processes and $\theta_1 = \theta_1(\theta_b)$. f_b does not depend on the angle $\tilde{\varphi}$ due

to the axial symmetry of the boundary conditions. Therefore Eq. (2.11) can be represented as:

$$\begin{aligned}
 n(\mathbf{r}_1, \theta_b) &= \int_0^{+\infty} \int_0^{2\pi} f_b(\theta_b, \tilde{w}_1, \theta_1(\theta_b)) \exp(-A(\mathbf{r}_1, \theta_b, \tilde{w}_1)) \tilde{w}_1^2 \sin(\tilde{\theta}_1) d\tilde{w}_1 d\tilde{\varphi} \\
 &= 2\pi \sin(\theta_1) \cdot \int_0^{+\infty} f_b(\theta_b, \tilde{w}_1, \theta_1(\theta_b)) \exp(-A(\mathbf{r}_1, \theta_b, \tilde{w}_1)) \tilde{w}_1^2 d\tilde{w}_1 \\
 &= 2\pi \sin(\theta_1) \cdot g(\mathbf{r}_1, \theta_b).
 \end{aligned}$$

The function $f_b(\theta_b, \tilde{w}_1)$ decreases with θ_b for each given value of \tilde{w}_1 , because at 90 AU $V_{z,H} \gg V_{\rho,H}$ and the distribution function has a maximum in the upwind direction. The loss-function, $A(\mathbf{r}_1, \theta_b, \tilde{w}_1)$, increases with θ_b for point 1 because the length of the trajectory has a minimal value upwind and $\exp(-A)$ decreases with θ_b . Hence, the function $g(\mathbf{r}_1, \theta_b)$ decreases with θ_b , and $\sin(\theta_1)$ increases with θ_b for $\theta_b \in [0, \pi/2]$. Therefore, $n(\mathbf{r}_1, \theta_b)$, that is a product of $\sin(\theta_1)$ and $g(\mathbf{r}_1, \theta_b)$, should have a maximum at a certain θ_b between 0° and 90° .

Figure 2.20a shows $n(\mathbf{r}_i, \theta_b)$ calculated numerically for point 1 in the upwind direction (curve 1) and for point 2 in the downwind direction (curve 2). The figure shows that the largest fraction of the interstellar atoms arrive at point 1 from $\theta \approx 15^\circ$ and at point 2 from $\theta \approx 55^\circ$. Therefore, contrary to expectations, most of the H atoms reach the vicinity of the Sun not exactly from the upwind direction.

Now, it is clear that the excess in the backscattered Lyman- α intensity in models 1 and 2 as compared with model 3 is related to the higher number densities of H atoms inside the heliosphere in models 1 and 2 arising from the lack of θ -dependent boundary conditions. In model 3, the number density at 90 AU decreases with θ .

It also becomes clear why the intensities (and line-shifts) of the radiation scattered by the primary interstellar atoms nearly coincide for all models as shown in Fig. 2.19b. This is because on the one hand, the angle-dependence of the hydrogen parameters at 90 AU for the primary interstellar atoms is weaker than for the secondary interstellar atoms. On the other hand, the distribution function of the primary interstellar atoms is closer to a Maxwellian than the distribution function of the secondary interstellar atoms.

From the middle column of Fig. 2.19a, c it can be seen that there are noticeable differences in the line-shifts of models 2 and 3 in the downwind direction. The differences are seen for the total radiation as well as for the radiation scattered by the secondary interstellar atoms. At the same time, there are almost no discrepancies in the line-shifts of model 1 and model 3, despite the fact that model 1 is the simplest model without any of the effects of the heliospheric interface. Therefore one would expect some differences.

In order to understand these results we calculated the contribution to the total radial velocity of hydrogen at point 2 (7 AU in downwind) from the particles that reach this point from different directions. Similar to $n(\mathbf{r}_i, \theta_b)$, the contribution to the radial velocity can be calculated as follows:

$$V_r(\mathbf{r}_i, \theta_b) = \frac{1}{\int_{-\infty}^{+\infty} f(\mathbf{r}_i, \mathbf{w}_i) d\mathbf{w}_i} \cdot \int_{\Omega_i} f(\mathbf{r}_i, \mathbf{w}_i) w_{i,r} d\mathbf{w}_i$$

Figure 2.20b shows $V_r(\mathbf{r}_i, \theta_b)$, calculated at point 2 for different models. It is seen that the maximum of $V_r(\mathbf{r}_i, \theta_b)$ is located approximately at $\theta=45^\circ$ for all models. However, model 2 (dashed curve in Fig. 3b) has a non-negligible contribution of negative values of $V_r(\mathbf{r}_i, \theta_b)$ for $\theta > 100^\circ$. The negative values of $V_r(\mathbf{r}_i, \theta_b)$ are due to relatively hotter secondary interstellar atoms in the downwind hemisphere (due to high temperature of the secondary interstellar atoms and absence of a decrease in the number density from upwind to downwind in model 2), which can reach point 2 from large values of angle θ . This makes the total line-shift of model 2 in the downwind region smaller as compared with models 1 and 3. The contributions of negative $V_r(\mathbf{r}_i, \theta_b)$ in model 1 and model 3 are smaller than in model 2, but due to different reasons. In model 3, the contribution of the particles with negative $V_r(\mathbf{r}_i, \theta_b)$ is significantly reduced because of the low number density of such particles at the outer boundary that comes from the self-consistent model results. As for model 1, we do not see this effect due to the relatively smaller temperature of the mixture of primary and secondary interstellar atoms as compared with the temperature of the secondary interstellar atoms, which exists in model 2.

Now let us consider the line-widths (right column in Fig. 2.19). Plot a demonstrates that there are essential qualitative differences in the line-widths calculated on the basis of the three models. Model 1 shows a monotonic increase in the line-width with θ . Model 2 shows a minimum of the line-width at $\theta \sim 60^\circ$. Model 3 shows a small local maximum at $\theta \sim 150^\circ$. These results demonstrate that the line-width of the backscattered Lyman- α profiles is very sensitive to the properties of the hydrogen distribution at the termination shock.

In the next section we will explain these qualitative differences and will show that the main cause of the difference is the kinetic non-Maxwellian nature of the hydrogen velocity distribution function at 90 AU. Note also that for the line-widths the simplified model 2a results are close to model 3 in the upwind hemisphere. However, large discrepancies in the downwind region still exist.

Now we will consider differences in the line-widths of the backscattered spectra calculated separately for the primary and secondary populations of H atoms (right columns of Fig. 2.19b, c). For both populations we observe large maxima in the line-widths at $\theta \sim 90^\circ$ in the results of model 3. Such strong maxima do not exist for model 2 and for model 2a. The latter means that the maxima are not due to the θ -dependence of the hydrogen parameters at 90 AU but rather to the non-Maxwellian velocity distribution function at the outer boundary. As was shown by Baranov et al. (1998) (see also, Izmodenov et al. 2001 and Fig. 3e, f of Katushkina and Izmodenov 2010) the components T_z and T_ρ of the kinetic temperatures calculated from the velocity distribution function of the interstellar hydrogen, i.e.

$$T_z(\mathbf{r}) \sim \int f(\mathbf{r}, \mathbf{w}) \cdot (V_z(\mathbf{r}) - w_z)^2 d\mathbf{w}$$

and

$$T_\rho(\mathbf{r}) \sim \int f(\mathbf{r}, \mathbf{w}) \cdot (V_\rho(\mathbf{r}) - w_\rho)^2 d\mathbf{w}$$

are fundamentally different from each other inside the heliosphere.

Table 2.3: Comparison of intensities, line-shifts and line-widths of the backscattered Lyman- α radiation for three models of the hydrogen distribution inside the heliosphere

$\theta = 0^\circ$	$I_{los}(R)$	V_{los} (km/s)	T_{los} (K)	$\frac{ I_{los}-I_{los,3} }{I_{los,3}}$	$\frac{ V_{los}-V_{los,3} }{V_{los,3}}$	$\frac{ T_{los}-T_{los,3} }{T_{los,3}}$
Model 1	677	-24.2	14,710	2.3	1.2	14.5
Model 2	720	-24.5	14,158	8.7	0.0	10.3
Model 3	662	-24.5	12,841	0.0	0.0	0.0
$\theta = 90^\circ$	$I_{los}(R)$	V_{los} (km/s)	T_{los} (K)	$\frac{ I_{los}-I_{los,3} }{I_{los,3}}$	$\frac{ V_{los}-V_{los,3} }{V_{los,3}}$	$\frac{ T_{los}-T_{los,3} }{T_{los,3}}$
Model 1	398	-0.9	17,505	4.7	200.0	18.0
Model 2	421	-0.6	15,561	10.8	100.0	4.9
Model 3	380	-0.3	14,834	0.0	0.0	0.0
$\theta = 180^\circ$	$I_{los}(R)$	V_{los} (km/s)	T_{los} (K)	$\frac{ I_{los}-I_{los,3} }{I_{los,3}}$	$\frac{ V_{los}-V_{los,3} }{V_{los,3}}$	$\frac{ T_{los}-T_{los,3} }{T_{los,3}}$
Model 1	127	20.3	18,984	24.5	1.4	11.3
Model 2	129	17.4	23,946	26.5	15.5	40.4
Model 3	102	20.6	17,060	0.0	0.0	0.0

See text for a description of the models. Fractional differences in intensity (columns 5–7) are shown as percentages

Recall that z-axis is the central axis of the axisymmetric heliosphere and ρ is the distance from that axis in a cylindrical coordinate system. In other words, the mean thermal velocities of the H atoms are different in different directions. Moreover, this difference between T_z and T_ρ temperatures increases approaching to the Sun due to local effects. The large maxima of the line-widths at $\theta = 90^\circ$ shown in Fig. 2.19b, c are related to the changes in the radial kinetic temperature T_r of the gas at 90 AU as a function of θ . For example, when an observer looks toward the upwind direction (i.e. $\theta = 0^\circ$) $T_r = T_z$, for a line-of-sight with $\theta = 90^\circ$ $T_r = T_\rho$ and for a line-of-sight of $\theta = 180^\circ$ $T_r = T_z$ again. In model 3 at the outer boundary, T_ρ is higher than T_z for each of the interstellar populations of H atoms based on the Baranov–Malama model results. This results in the maxima of T_r at $\theta = 90^\circ$ and it is reflected in the maxima of the line-widths for the photons scattered by each population of interstellar H atoms separately.

The differences in the Lyman- α intensities, line-shifts, and line-widths calculated in models 1–3 are summarized in Table 2.3. It shows the differences (both absolute and relative) between the model results for the upwind ($\theta = 0^\circ$), crosswind ($\theta = 90^\circ$), and downwind ($\theta = 180^\circ$) directions. It shows that the one-component hot model 1 gives differences from 2% (in the upwind direction) to 24% (in the downwind direction) as compared with model 3 in intensities and about 10–18% difference in the line-widths. The two-component hot model 2 leads to 8–27% discrepancies with model 3 in the intensities, and from 10% (upwind) to 40% (downwind) discrepancies in the line-widths. The differences in the line-shifts of models 1 and 2 relative to model 3 are also large, especially for the crosswind direction. However, they are related to very small values of the line-shifts and most probably can not be detected experimentally.

Line-Width of the Backscattered Lyman- α Profile as a Diagnostic of the Nature of the Heliospheric Interface

Costa et al. (1999) and Quémerais et al. (2006) have analyzed the spectral properties of the backscattered solar Lyman- α radiation measured by SOHO/SWAN in 1996–2003. The Lyman- α line-width as a function of line-of-sight direction was studied. It was shown that there is a noticeable minimum in the line-width at $\theta = 50^\circ - 60^\circ$. This minimum was interpreted as an indication of the two (primary and secondary) components of the interstellar H atoms in the heliosphere and, therefore, as evidence of the heliospheric interface. Indeed, the results obtained in the frame of the one-component classical hot model shows (dashed-dot curve in Fig. 2.19a) a monotonic increase of the line-width from upwind to downwind. The existence of the two components, which have the bulk velocities shifted with respect to each other, can help to produce the minimum of the line-width in directions close to the crosswind direction.

Models 2 and 3 described in this paper have two populations of H atoms at the outer boundary at 90 AU. Therefore, one can expect that a minimum of the line-widths should be obtained in these models. However, as Fig. 2.19a shows, the minimum is seen only for model 2 and not for model 3. Instead, for model 3 we see a small maximum in temperature at $\theta = 150^\circ$. In order to explain these features we have performed a series of additional test calculations.

Our goal is to understand and distinguish the roles of different effects influencing the line-width of Lyman- α profiles. To do that we studied the effects of all possible model parameters and established that the following factors contribute to the dependence of the line-width (T_{los}) on the angle θ :

1. The ionization processes that change the parameters of H atoms near the Sun. From our test calculations we have found that solar gravitation and radiation pressure have a smaller influence on the line-width than ionization.
2. The existence of two populations of the interstellar hydrogen atoms that are shifted in velocity space. This effect leads to the appearance of the minimum of T_{los} at $\theta = 90^\circ$, as discussed before.
3. The non-Maxwellian behavior of the velocity distribution function of the two populations of hydrogen at 90 AU, or more precisely, the large difference between the T_z and T_ρ “temperature” components (z and ρ are cylindrical coordinates). This effect exists for model 3.
4. The spectral shape of the solar Lyman- α line. It will be shown below that the shape of the solar spectrum has some small but interesting effect on the line-width as a function of θ .

Figure 2.22 summarizes the results of the test calculations and explores the effects listed above. Table 2.2 spells out the model numbering scheme used in Fig. 2.22. For all of the calculations in this section, we assume that the solar gravitational force is in balance with solar radiation pressure, i.e. $\mu = 1$ and the trajectories of the H atoms are straight lines. To explore the effects of ionization

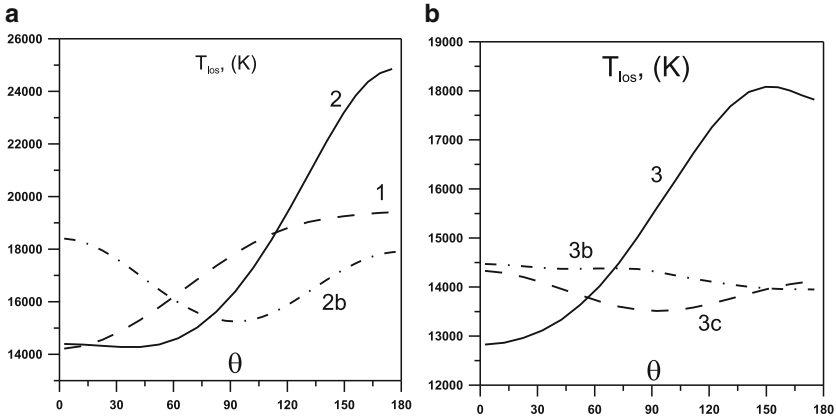


Figure 2.22: Results of test calculations of the Lyman- α line-width as a function of angle θ . Model numbers are described in Table 2.2. Results are based on the one-component hot model (model 1 curve 1) and the two-component hot model (model 2 curves 2 and 2b) are shown in plot (a) and results based on model 3 (curves 3, 3b, 3c) are shown in plot (b). Curves 2 and 2b correspond to calculations based on model 2 with and without ionization; curve 3 corresponds to model 3, and curve 3b and 3c are the results of model 3, where ionization was switched off. In all calculations except model 3c, the solar spectrum from Lemaire et al. (1998) was assumed. For model 3c, a flat solar spectrum was employed [From Katushkina and Izmodenov (2011)]

in the vicinity of the Sun, we performed test calculations with a typical ionization rate of $\beta_E = 5.9 \times 10^{-7} \text{ s}^{-1}$ as well as calculations with $\beta_E = 0$ (models 2b, 3b, 3c).

The effects of the local ionization on the function of $T_{los}(\theta)$ are clearly illustrated in the frame of the one-component hot model 1 (curve 1 in Fig. 2.22a) since neither the two-component nor the non-Maxwellian effects are taken into account in this model. The line-width of the backscattered Lyman- α profile increases monotonically from the upwind direction to downwind. This behavior reflects the angular variation in the effective radial temperature of the H atoms that increases from upwind to downwind (see Fig. 3.5 in Izmodenov 2006). Such a behavior is due to a combination of the so-called selection effect that leads to a reduction in the atom temperature in the upwind direction and in the effect of broadening of the velocity distribution function toward the downwind direction. The latter effect is due to the fact that atoms penetrate into the downwind direction mainly from the sides that makes the distribution function broader (see Fig. 3.4 in Izmodenov 2006). The selection effect is the effect when the slower atoms are more ionized as compared with the fast atoms, because they spend more time before approaching the vicinity of the Sun (and Earth) and have more time to be ionized. For a more detailed description of these effects and evolution of the H atom velocity distribution inside the heliosphere, see Izmodenov (2006).

Results of the two-component hot model, 2b, that do not account for the ionization (curve 2b in Fig. 2.22) illustrate the effect of the two populations of the interstellar H atoms. These two populations have different bulk velocities V_z (at 90 AU in the upwind direction: $V_{z,primary} \approx -27$ km/s and $V_{z,secondary} \approx -16$ km/s) and rather small thermal velocities. Therefore, in the upwind and downwind directions (where $V_r = \pm V_z$), the line-of-sight projections of the velocity distribution functions of the primary and secondary components overlap only partially in velocity space. In the crosswind direction $V_r = V_\rho \approx 0$ for both primary and secondary interstellar atoms. This means that in this direction the projections of the distribution functions on the radial line-of-sight overlap completely. That is why the radial temperature of the mixture of primary and secondary interstellar atoms is smaller in the crosswind direction than in the upwind and downwind directions. This minimum of the radial temperature of H atoms in the crosswind direction is reflected in the Lyman- α line-widths as seen from model 2b.

Results of the two-component hot model, curve 2 of Fig. 2.22, where the ionization is taken into account combine both the increase in T_{los} from upwind to downwind due to the ionization effect and the local minimum in the crosswind direction due to the two populations of H atoms. Hence, a small minimum of T_{los} at $\theta = 50\text{--}60^\circ$ is seen in curve 2.

The line-width obtained from model 3 is presented in Fig. 2.22b. Note that this model takes into account all known effects of the heliospheric interface, namely: (1) two populations of interstellar H atoms, (2) θ -dependence of the hydrogen parameters at 90 AU, and (3) non-Maxwellian features of the hydrogen velocity distribution function at the outer boundary of the model. In particular, the differences between kinetic temperature's components, T_z and T_ρ , play an important role.

Curves 3b and 3c correspond to models that do not take ionization into account. Additionally, model 3c assumes that the solar Lyman- α flux does not depend on frequency. This case is referred to as the “flat” solar spectrum. Note that in all the other models we use the shape of the solar spectrum from Lemaire et al. (1998).

It can be seen that the effect of minimum in T_{los} at $\theta = 90^\circ$ (due to the two populations) almost disappears in model 3c, but is still visible. This disappearance of the minimum is related to the growth of the radial kinetic temperature T_r with an increase of θ at 90 AU. The effect of the T_r increase with θ compensates the effect of the minimum in the radial hydrogen temperature in crosswind due to the two populations of H atoms. That is why the value of the minimum of the line-widths at $\theta = 90^\circ$ is much smaller for model 3c as compared with model 2b.

It is interesting to note that for model 3b (which is more realistic than model 3c) the local minimum of T_{los} at $\theta = 90^\circ$ is replaced with a small maximum. This effect is due to the shape of the solar spectrum. Remember that in model 3c we use a flat solar spectrum while in model 3b we use the nonuniform solar spectra from Lemaire et al. (1998).

Let us return to model 3 without any additional assumptions. It is seen (curve 3) that in this case there is no minimum in T_{los} at $50\text{--}60^\circ$ at all, but instead a small maximum at $\theta = 150^\circ$. This maximum can be explained by the θ -dependence of the hydrogen kinetic temperature T_r . The radial temperature of the sum of the primary and secondary interstellar atoms is shown in Fig. 2.23 (plot a corresponds to model 2, plot b corresponds to model 3). It is seen that in the case of the two-

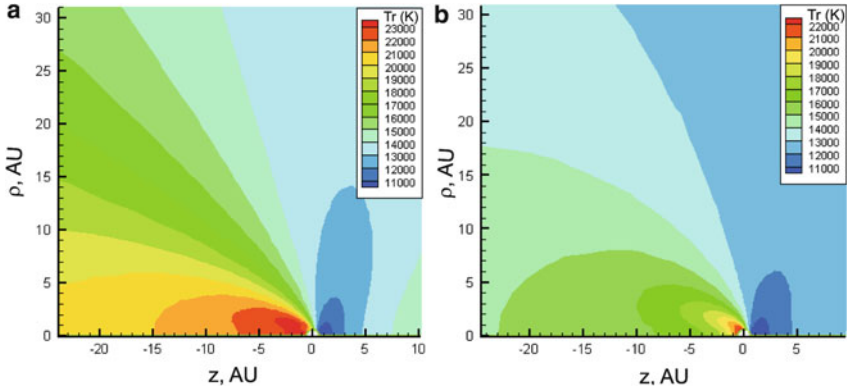


Figure 2.23: Kinetic radial temperature (T_r) for the sum of the primary and secondary interstellar atoms in the heliosphere; Plot **a** corresponds to the two-component hot model 2, plot **b** corresponds to the results of the model 3. In these calculations $\mu = 1$ and $\beta_E = 5.9 \times 10^{-7} \text{ s}^{-1}$ [From [Katushkina and Izmodenov \(2011\)](#)]

component hot model 2 ionization leads to the maximum of T_r in downwind. For model 3 the maximum of T_r is located at about $\theta = 150^\circ$. This effect is reflected in the line-widths of the Lyman- α radiation that is seen in curve 3 of Fig. 2.22b.

Summary of the Section

In this section we employed various models of hydrogen distribution in the heliosphere to compute the spectral properties of the backscattered solar Lyman- α radiation as it would be measured at 1 AU in the anti-solar directions. We have found that imprints of the heliospheric interface in the H atom distribution inside the heliosphere have a strong influence on the Lyman- α parameters.

We considered the minimum of the line-width of the backscattered Lyman- α radiation at $50\text{--}60^\circ$ from upwind that was observed by SWAN ([Costa et al. 1999](#); [Quémerais et al. 2006](#)). In the experimental data the line-width in the directions of $\theta = 50\text{--}60^\circ$ is smaller than in the upwind direction by 1,500–2,000 K. This minimum is seen for 1996 and 1997 and practically not seen for 2002–2003 years although data points for small angles are not available for this period (see Fig. 7 in [Quémerais et al. 2006](#)). This minimum was explained in [Costa et al. \(1999\)](#) and [Quémerais et al. \(2006\)](#) by the existence of two different populations of interstellar hydrogen atoms that are shifted in velocity space. However, we noticed that the line-width calculated with the 2D stationary Baranov–Malama model ([Quémerais and Izmodenov 2002](#)) has no minimum of T_{los} . The non-stationary 2D Baranov–Malama model ([Quémerais et al. 2008](#)) predicts a small minimum in 2003, but no minimum in 1997.

In this work we explored theoretically the nature of the observed minimum in T_{los} on the basis of three cases of hydrogen distribution inside the heliosphere. It

was shown that the minimum of the line-widths appears only for the two-component hot model, and there is no minimum at all for model 3 that takes into account all effects of the heliospheric interface. It was found that the absence of the minimum in model 3 is due to the effect of the two components being compensated by the non-Maxwellian features of the velocity distribution of H atoms at 90 AU after they passed the heliospheric interface region, namely, by a strong anisotropy of the kinetic temperatures of H atoms ($T_z < T_\rho$).

Therefore, the question of why the minimum of the Lyman- α line-width exists in the experimental data remains unanswered. Possibilities for reproducing the minimum still exist in the context of model 3. Firstly, the models considered here do not take into account the effects of latitudinal and solar cycle variations of the photoionization and charge exchange rates as well as solar radiation pressure. These local effects may potentially change the result of this paper.

Another option to explain the minimum in line-width would be to change the boundary conditions at 90 AU, i.e. to make a change in the model of the heliospheric interface. For example, interstellar magnetic field may play a key role (Izmodenov et al. 2005). Another possibility is a change in the multi-component nature of both the heliospheric and interstellar plasmas (Malama et al. 2006; Izmodenov et al. 2009; Chalov et al. 2010). In this non-equilibrium plasma model the interstellar pickup ions would be treated as a separate kinetic component. The plasma temperature in the vicinity of the heliopause is smaller in that model as compared with the Baranov–Malama model. Therefore, we could expect a decrease in the kinetic temperatures of the secondary interstellar atoms. This might result in a larger velocity space separation of the primary and secondary interstellar atoms at 90 AU. The separation may enhance the effect of the two populations. As a result one may hope that the observed minimum will appear in the model.

Summary

The interaction between the supersonic flow of partially ionized plasma of the local interstellar medium and the solar wind produces a complicated flow pattern consisting of one or two shock waves (the heliospheric termination shock and, possibly, the bow shock in the LISM), and a contact discontinuity, the heliopause. Due to the charge exchange process, the region between the two shocks (heliospheric interface) separating these flows plays the role of a filter for the penetration of the interstellar hydrogen atoms (and also for O, N, and other species) into the Solar System.

From a theoretical point of view, the interaction should be considered in the frame of kinetic-continuum models where the interstellar H atom component is described in the framework of kinetic theory, since for hydrogen atoms the Knudsen number with respect to charge exchange is $\text{Kn} \sim 1$. The first self-consistent model of the SW/LIC interaction was developed by Baranov and Malama (1993). Since that time the set of kinetic-continuum models was developed. The modern kinetic-continuum models take into account the following physical components/effects:

- Ionized interstellar helium component and solar wind alpha particles;
- Anomalous and galactic cosmic rays;

- Interstellar magnetic field;
- Solar cycle variations of the solar wind parameters;
- The heliotail;
- Filtration of interstellar oxygen and nitrogen;
- The multi-component nature of the heliospheric plasma.

Extensive efforts by other groups have also been put into modelling the heliospheric interface (Opher et al. 2009; Heerikhuizen and Pogorelov 2011; and references therein). Nevertheless, the complete time-dependent multi-component kinetic-continuum model that includes all effects above (plus the interplanetary magnetic field) simultaneously has not yet been developed. This leaves a challenge for future theoretical studies.

The numerical kinetic-continuum models of the heliospheric interface in the frame of the Baranov–Malama model led, first, to the prediction of the many physical phenomena discovered later onboard spacecraft and, secondly, to the interpretation of previously obtained experimental data. In December 2004, an event expected for more than 30 years took place: the Voyager 1 spacecraft finally crossed the heliospheric termination shock at a distance of 94 AU. This was predicted (with a 10 % accuracy) more than 25 years ago (Baranov et al. 1981; Baranov 1990, 2002).

In spite of significant progress in recent years, the global self-consistent 3D models are too computationally expensive to routinely perform detailed calculations of the velocity distribution function in the vicinity of the Sun that is needed for analysis of the backscattered Lyman- α radiation. Katushkina and Izmodenov (2010, 2011) have developed a model which combines the simplicity of the hot-type models of the H atom distribution inside the heliosphere with the results of a global model of the SW/LIC interaction. It has been shown that this newly developed model can be used for modeling the velocity distribution of the interstellar atoms inside the heliosphere with sufficient accuracy. This model has been used to analyze how the imprint of the heliospheric interface in the velocity distribution of the interstellar hydrogen can be seen at one or several AU. We have also demonstrated that the imprint of the heliospheric interface in the H atom distribution inside the heliosphere can have a strong influence on the observed backscattered Lyman- α parameters. It has been shown that the theoretically calculated moments of the Lyman- α spectra have in general very good agreement with the SOHO/SWAN data. However, some measured spectral features can not be reproduced by the current model.

One such feature that is not reproduced by the model is the minimum of the line-width of the backscattered Lyman- α radiation at 50–60° from the upwind direction that was observed by SWAN (Costa et al. 1999; Quémerais et al. 2006). This minimum is supposed to be a natural consequence of there being two (primary and secondary) populations of H atoms in the heliosphere. However, the non-Maxwellian features of the H atom velocity distribution at 90 AU makes the effect of the minimum non-visible in any model that assumes the velocity distribution function at 90 AU to be in accordance with the Baranov–Malama (1993) model.

Overall, from the results reviewed and presented in the paper we can conclude the following:

- Backscattered solar Lyman- α and its spectral characteristics like line-widths are an excellent tool to explore kinetic properties of the interstellar atoms, and, therefore, a tool to study the region of the SW/LIC interaction.
- Our state-of-the-art model ([Katushkina and Izmodenov 2011](#)) has been developed specifically to model the distribution of H atoms inside the heliosphere properly for the purpose of understanding the spectral parameters of the backscattered solar Lyman- α . This model allows us to combine the simplicity of the hot-type models of the H atom distribution inside the heliosphere with the results of the global models of the SW/LIC interaction.
- The comparison of the theoretically calculated Lyman- α intensities, line-shifts and line-widths with SOHO/SWAN measurements have shown quite good agreement.
- Solar cycle variations of the solar wind parameters influences the H atom distribution and should be taken into account in the analysis of backscattered Lyman- α .
- The qualitative difference in the line-width minimum measured at $\sim 60^\circ$ discussed in this paper could be explained by the effects of the interstellar/interplanetary magnetic fields or by the effects of the non-thermal behavior of the interstellar plasma component. The exploration of these effects is the subject for further studies.

Acknowledgements

The authors would like to thank ISSI for their support of the working group. The calculations were performed by using the supercomputers of the Russian Academy of Sciences and Lomonosov Moscow State University (“Lomonosov” and “Chebishev”). The work was performed under the Presidium RAS Programm 22. V.I. and O.K. were partially supported by RFBR grants 10-02-93113-CNRS-a, 10-02-01316-a, 11-02-92605-RS-a, and the Regional Public Fund for Russian science. M.B. acknowledges support from the Polish ministry for science and higher education, grants NS-1260-11-09 and N-N203-513-038.

Bibliography

- J.M. Ajello, A.I. Stewart, G.E. Thomas, A. Graps, Solar cycle study of interplanetary Lyman-alpha variations: Pioneer Venus Orbiter sky background results. *Astrophys. J.* **317**, 964–986 (1987)
- D.B. Aleksashov, V. Baranov, E. Barsky, A. Myasnikov, An axisymmetric magnetohydrodynamic model for the interaction of the solar wind with the local interstellar medium. *Astron. Lett.* **26**, 743–749 (2000)
- I.I. Alekseev, A.P. Kropotkin, Passage of energetic particles through a magnetohydrodynamic discontinuity surface. *Geomagn. Aeron.* **10**, 755 (1971)
- D.B. Alexashov, V.V. Izmodenov, M. Opher, Effects of the heliospheric and interstellar magnetic field on the heliospheric interface. 37th COSPAR Scientific Assembly D13-0015-08, P025-TueWed (poster) (2008)

- W.I. Axford, The interaction of the solar wind with the interstellar medium. In *Solar wind*, ed. by C.P. Sonett, P.J. Coleman, J.M. Wilcox. (Scientific and Technical Information Office, National Aeronautics and Space Administration, Washington), p. 609 *format?* (1972)
- W.I. Axford, A.J. Dessler, B. Gottlieb, Termination of solar wind and solar magnetic field. *Astrophys. J.* **137**, 1268–1278 (1963)
- V.B. Baranov, Gasdynamics of the solar wind interaction with the interstellar medium. *Space Sci. Rev.* **52**, 89–120 (1990)
- V.B. Baranov, The heliosheath as a special case of starsheaths and the hydrogen wall as a signature of the heliosheath. *Planet. Space Sci.* **50**, 535–539 (2002)
- V.B. Baranov, M.K. Ermakov, M.G. Lebedev, A three-component model of solar wind-interstellar medium interaction: some numerical results. *Sov. Astron. Lett.* **7**, 206–209 (1981)
- V.B. Baranov, V.V. Izmodenov, Y.G. Malama, On the distribution function of H atoms in the problem of the solar wind interaction with the local interstellar medium. *J. Geophys. Res.* **103**, 9575–9586 (1998)
- V.B. Baranov, K.V. Krasnobaev, A.G. Kulikovskiy, *Sov. Phys. Dokl.* **15**, 791 (1971)
- V.B. Baranov, M.G. Lebedev, Y.G. Malama, The influence of the interface between heliosphere and the local interstellar medium on the penetration of the H-atoms to the solar system. *Astrophys. J.* **375**, 347–351 (1991)
- V.B. Baranov, Y.G. Malama, Model of the solar wind interaction with the local interstellar medium: numerical solution of self-consistent problem. *J. Geophys. Res.* **98**, 15157–15163 (1993)
- V.B. Baranov, Y.G. Malama, Axisymmetric self-consistent model of the solar wind interaction with the LISM: basic results and possible ways of development. *Space Sci. Rev.* **78**, 305–316 (1996)
- V.B. Baranov, N.A. Zaitsev, On the problem of the solar wind interaction with magnetized interstellar plasma. *Astron. Astrophys.* **304**, 631–637 (1995)
- C.A. Barth, Mariner 6 measurements of the Lyman α sky background. *Astrophys. J. Lett.* **161**, L181–L184 (1970)
- J.-L. Bertaux, J.E. Blamont, Evidence for a source of an extraterrestrial hydrogen Lyman α emission: the interstellar wind. *Astron. Astrophys.* **11**, 200 (1971)
- J.-L. Bertaux, R. Lallement, Analysis of interplanetary Lyman α line profile with a hydrogen absorption cell: theory of the Doppler angular spectral scanning method. *Astron. Astrophys.* **140**, 230–242 (1984)
- J.-L. Bertaux, A. Ammar, J.E. Blamont, OGO-5 determination of the local interstellar wind parameters. *Space Res.* **12**, 1559–1567 (1972)
- J.-L. Bertaux, J.E. Blamont, N. Tabarie, W.G. Kurt, M.C. Bourgin, A.S. Smirnov, N.N. Dementeva, Interstellar medium in the vicinity of the sun: a temperature measurement obtained with the Mars-7 interplanetary probe. *Astron. Astrophys.* **46**, 19–29 (1976)
- J.L. Bertaux, J.E. Blamont, E.N. Mironova, V.G. Kurt, M.C. Bourgin, Temperature measurement of interplanetary interstellar hydrogen. *Nature* **270**, 156–158 (1977)
- J.-L. Bertaux, E. Quémerais, R. Lallement, E. Kyrölä, W. Schmidt, T. Summanen, J.P. Goutail, M. Berthé, J. Costa, T. Holzer, First results from the SWAN Lyman α solar wind mapper on SOHO. *Sol. Phys.* **175**, 737–770 (1997)
- J.-L. Bertaux, E. Kyrölä, E. Quémerais, R. Lallement, W. Schmidt, T. Summanen, J. Costa, T. Mäkinen, SWAN observations of the solar wind latitude distribution and its evolution since launch. *Space Sci. Rev.* **87**, 129–132 (1999)
- P.W. Blum, H.-J. Fahr, Interaction between interstellar hydrogen and the solar wind. *Astron. Astrophys.* **4**, 280–290 (1970)
- P.W. Blum, J. Pfeleiderer, C. Wulf-Mathies, Neutral gases of interstellar origin in interplanetary space. *Planet. Space Sci.* **23**, 93–105 (1975)
- P. Blum, P. Gangopadhyay, H.S. Ogawa, D.L. Judge, Solar-driven neutral density waves. *Astron. Astrophys.* **272**, 549–554 (1993)
- J.C. Brandt, J.W. Chamberlain, Interplanetary gas. I. hydrogen radiation in the night sky. *Astrophys. J.* **130**, 670–682 (1959)

- P.C. Brandt, E.C. Roelof, P. Wurz, S. Barabash, D. Bazell, R. DeMajistre, T. Sotirelis, R. Decker, Energetic neutral atom (ENA) imaging of the heliosheath: spectral characteristics and implications for shock acceleration from observations by the neutral particle detector (NPD) on board Venus Express (VEX). American Geophysical Union, Spring Meeting, abstract SH24A-01 (2009)
- L.F. Burlaga, N.F. Ness, M.H. Acuña, Crossing the termination shock into the heliosheath: magnetic fields. *Science* **309**, 2027–2029 (2005). doi:10.1126/science.1117542
- M. Bzowski, Response of the groove in heliospheric Lyman-alpha glow to latitude-dependent ionization rate. *Astron. Astrophys.* **408**, 1155–1164 (2003)
- M. Bzowski, Survival probability and energy modification of hydrogen energetic neutral atoms on their way from the termination shock to Earth orbit. *Astron. Astrophys.* **488**, 1057–1068 (2008)
- M. Bzowski, D. Ruciński, Solar cycle modulation of the interstellar hydrogen density distribution in the heliosphere. *Space Sci. Rev.* **72**, 467–470 (1995)
- M. Bzowski, H.-J. Fahr, D. Ruciński, H. Scherer, Variation of bulk velocity and temperature anisotropy of neutral heliospheric hydrogen during the solar cycle. *Astron. Astrophys.* **326**, 396–411 (1997)
- M. Bzowski, T. Summanen, D. Ruciński, E. Kyrölä, Response of interplanetary glow to global variations of hydrogen ionization rate and solar Lyman α flux. *J. Geophys. Res.* **107**, CiteID 1101 (2002). doi:10.1029/2001JA000141
- M. Bzowski, T. Makinen, E. Kyrölä et al., Latitudinal structure and north-south asymmetry of the solar wind from Lyman-alpha remote sensing by SWAN. *Astron. Astrophys.* **408**, 1165–1177 (2003)
- M. Bzowski, E. Möbius, S. Tarnopolski et al., Density of neutral interstellar hydrogen at the termination shock from Ulysses pickup ion observations. *Astron. Astrophys.* **491**, 7–19 (2008)
- S.V. Chalov, H.-J. Fahr, Energetic particles from the outer heliosphere appearing as a secondary pick-up ion component. *Astron. Astrophys.* **401**, L1–L4 (2003)
- S.V. Chalov, D.B. Alexashov, D. McComas et al., Scatter-free pickup ions beyond the heliopause as a model for the interstellar boundary explorer ribbon. *Astrophys. J. Lett.* **716**, L99–L102 (2010)
- J. Costa, R. Lallement, E. Quémerais et al., Heliospheric interstellar H temperature from SOHO/SWAN H cell data. *Astron. Astrophys.* **349**, 660–672 (1999)
- J.M.A. Danby, G.L. Camm, Stat. dynam. accretion Monthly Not. Royal Astron. Soc. **117**, 50–71 (1957)
- L. Davis Jr., Interplanetary magnetic fields and cosmic rays. *Phys. Rev.* **100**, 1440–1444 (1955). doi:10.1103/PhysRev.100.1440
- R.B. Decker, S.M. Krimigis, E.C. Roelof et al., Voyager 1 in the foreshock, termination shock, and heliosheath. *Science* **309**, 2020–2024 (2005)
- H.-J. Fahr, On the influence of the neutral interstellar matter on the upper atmosphere. *Astrophys. Space Sci.* **2**, 474–495 (1968a)
- H.-J. Fahr, Neutral corpuscular energy flux by charge transfer collisions in the vicinity of the Sun. *Astrophys. Space Sci.* **2**, 496–503 (1968b)
- H.-J. Fahr, The interplanetary hydrogen cone and its solar cycle variations. *Astron. Astrophys.* **14**, 263–274 (1971)
- H.-J. Fahr, The extraterrestrial UV-background and the nearby interstellar medium. *Space Sci. Rev.* **15**, 483–540 (1974)
- H.-J. Fahr, Change of interstellar gas parameters in stellar-wind-dominated astrospheres: the solar case. *Astron. Astrophys.* **66**, 103–117 (1978)
- W.C. Feldman, J.J. Lange, F. Scherb, Interstellar helium in interplanetary space. In *Solar Wind*, ed. by C.P. Sonett, P.J. Coleman, J.M. Wilcox. (Scientific and Technical Information Office, National Aeronautics and Space Administration, Washington, 1972), p. 668
- H.O. Funsten, F. Allegrini, G.B. Crew et al., Structures and spectral variations of the outer heliosphere in IBEX energetic neutral atom maps. *Science* **326**, 964 (2009)

- S.A. Fuselier, F. Allegrini, H.O. Funsten et al., Width and variation of the ENA flux ribbon observed by the interstellar boundary explorer. *Science* **326**, 962 (2009)
- K. Gringauz, V. Bezrukih, V. Ozerov, R. Ribchinsky, A study of the interplanetary ionized gas, high-energy electrons and corpuscular radiation from the Sun by means of the three-electrode trap for charged particles on the second soviet cosmic rocket. *Sov. Phys. Doklady* **5**, 361 (1960)
- M. Gruntman, V.V. Izmodenov, Mass transport in the heliosphere by energetic neutral atoms. *J. Geophys. Res.* **109**, A12108 (2004). doi:10.1029/2004JA010727
- M. Gruntman, E.C. Roelof, D.G. Mitchell, H.-J. Fahr, H.O. Funsten, D.J. McComas, Energetic neutral atom imaging of the heliospheric boundary region. *J. Geophys. Res.* **106**, 15767–15782 (2001)
- J. Heerikhuisen, N.V. Pogorelov, An estimate of the nearby interstellar magnetic field using neutral atoms. *Astrophys. J.* **738**, 29 (2011). doi:10.1088/0004-637X/738/1/29
- M. Hilchenbach, K.C. Hsieh, D. Hovestadt et al., Detection of 55–80 keV hydrogen atoms of heliospheric origin by CELIAS/HSTOF on SOHO. *Astrophys. J.* **503**, 916–922 (1998)
- M. Hilchenbach, K.C. Hsieh, D. Hovestadt, R. Kallenbach, A. Czechowski, E. Möbius, P. Bochsler, Energetic neutral hydrogen of heliospheric origin observed with SOHO/CELIAS at 1 AU. In *The Outer Heliosphere: The Next Frontiers*, ed. by K. Scherer, H. Fichtner, H.J. Fahr, E. Marsch. (Pergamon, Elmsford, 2000), pp. 273–276
- A.J. Hundhausen, Interplanetary neutral hydrogen and the radius of the heliosphere. *Planet. Space Sci.* **16**, 783–793 (1968)
- P.A. Isenberg, Evolution of interstellar pickup ions in the solar wind. *J. Geophys. Res.* **92**, 1067–1073 (1987)
- V.V. Izmodenov, Physics and gasdynamics of the heliospheric interface. *Astrophys. Space Sci.* **274**, 55–69 (2000)
- V.V. Izmodenov, Velocity distribution of interstellar H atoms in the heliospheric interface. *Space Sci. Rev.* **97**, 385–388 (2001)
- V.V. Izmodenov, Early concepts of the heliospheric interface: H atoms. In *The Physics of the Heliospheric Boundaries*, ed. by V.V. Izmodenov, R. Kallenbach. ISSI Scientific Report No. 5 (ESA-ESTEC, Paris, 2006), pp. 45–65
- V.V. Izmodenov, Local interstellar parameters as they are inferred from analysis of observations inside the heliosphere. *Space Sci. Rev.* **143**, 139–150 (2009)
- V.V. Izmodenov, D. Alexashov, A model for the tail region of the heliospheric interface. *Astronomy Lett.* **29**, 58–63 (2003)
- V.V. Izmodenov, D. Alexashov, Kinetic vs multi-fluid models of H atoms in the heliospheric interface. In *Solar Wind 11 / SOHO 16 Connecting Sun and Heliosphere conference*, ed. by B. Fleck, T.H. Zurbuchen, H. Lacoste. (ESA SP-592, 2005), p. 355
- V.V. Izmodenov, D. Alexashov, Multi-component 3d modeling of the heliospheric interface: effects of interstellar magnetic field. In *Physics of the inner heliosheath: Voyager observations, theory, and future prospects*. 5th annual IGPP international astrophysics conference. AIP Conference Proceedings, vol. 858 (2006), pp. 14–19
- V.V. Izmodenov, Y.G. Malama, A.P. Kalinin et al., Hot neutral H in the heliosphere: elastic H-H, H-p collisions. *Astrophys. Space Sci.* **274**, 71–76 (2000)
- V.V. Izmodenov, M. Gruntman, Y.G. Malama, Interstellar hydrogen atom distribution function in the outer heliosphere. *J. Geophys. Res.* **106**, 10681 (2001)
- V.V. Izmodenov, G. Gloeckler, Y.G. Malama, When will Voyager 1 and 2 cross the termination shock? *Geophys. Res. Lett.* **30**, 3–1 (2003). doi:10.1029/2002GL016127
- V.V. Izmodenov, D. Alexashov, A. Myasnikov, Direction of the interstellar H atom inflow in the heliosphere: role of the interstellar magnetic field. *Astron. Astrophys.* **437**, L35–L38 (2005)
- V.V. Izmodenov, Y.G. Malama, M.S. Ruderman, Modeling of the outer heliosphere with the realistic solar cycle. *Adv. Space Res.* **41**, 318–324 (2008)
- V.V. Izmodenov, Y.G. Malama, M.S. Ruderman et al., Kinetic-gasdynamic modeling of the heliospheric interface. *Space Sci. Rev.* **146**, 329–351 (2009)
- J.A. Joselyn, T.E. Holzer, The effect of asymmetric solar wind on the Lyman α sky background. *J. Geophys. Res.* **80**, 903–907 (1975)

- O.A. Katushkina, V.V. Izmodenov, Effect of the heliospheric interface on the distribution of interstellar hydrogen atom inside the heliosphere. *Astronomy Lett.* **36**, 297–300 (2010)
- O.A. Katushkina, V.V. Izmodenov, The influence of effects on the heliospheric interface on parameters of backscattered solar $L\alpha$ radiation measured at the Earth's orbit. *Cosmic Res.* **50**, 141–151 (2012)
- S.M. Krimigis, D.G. Mitchell, E.C. Roelof, P.C. Brandt, Energetic neutral atoms (ENA) from the termination shock/heliosheath? the view from 10AU. Paper presented at Voyagers in the heliosheath: observations, models, and plasmas physics Kauai, Hawaii, 9–14 Jan 2009
- S.M. Krimigis, E.C. Roelof, R.B. Decker, M.E. Hill, Zero outward flow velocity for plasma in a heliosheath transition layer. *Nature* **474**, 359–361 (2011)
- S. Kumar, A.L. Broadfoot, Evidence from Mariner 10 of solar wind flux depletion at high ecliptic latitudes. *Astron. Astrophys.* **69**, L5–L8 (1978)
- S. Kumar, A.L. Broadfoot, Signatures of solar wind latitudinal structure in interplanetary Lyman α emissions: Mariner 10 observations. *Astrophys. J.* **228**, 302–311 (1979)
- J.E. Kupperian, E.T. Byram, T.A. Chubb, H. Friedman, Far ultraviolet radiation in the night sky. *Planet. Space Sci.* **1**, 3–6 (1959)
- V.G. Kurt, Measurement of scattered Lyman α radiation in the vicinity of the Earth and in interplanetary space. In *Space Research: Transactions of the All-union Conference on Space Physics*, ed. by G.A. Skuridin et al. NASA Technical Translation: NASA TT F-389, Science Publishing House, Moscow, 10–16 June 1965, p. 769 (Translation published by NASA, Washington DC, USA, May 1966)
- V.G. Kurt, Kosmicheskie Issledovania (in russian) **5**(6), 769–775 (1967)
- V.G. Kurt, T.A. Germogenova, Scattering of solar Lyman α radiation by galactic hydrogen. *Sov. Astron.* **11**, 278–282 (1967)
- V.G. Kurt, R.A. Syunyaev, Observations and interpretation of the ultraviolet radiation of the Galaxy. *Sov. Astron.* **11**, 928–931 (1967)
- E. Kyrölä, T. Summanen, P. Raback, Solar cycle and interplanetary hydrogen. *Astron. Astrophys.* **288**, 299–314 (1994)
- R. Lallement, The interaction of the heliosphere with interstellar medium. In *The Century of Space Science*, ed. by A.M. Bleeker, J. Geiss, M.C.E. Huber. (Kluwer, New York, 2001), pp. 1191–1216
- R. Lallement, J.-L. Bertaux, Deceleration of interstellar hydrogen at heliopause crossing suggested by Lyman-alpha spectral observations. *Astron. Astrophys.* **231**, L3–L6 (1990)
- R. Lallement, A.I.F.S. Stewart, Out-of-ecliptic Lyman α observations with Pioneer-Venus: solar wind anisotropy degree in 1986. *Astron. Astrophys.* **227**, 600–608 (1990)
- R. Lallement, J.-L. Bertaux, V.G. Kurt, E.N. Mironova, Observed perturbations of the velocity distribution of interstellar H atoms in the solar system with Prognoz Lyman α measurements. *Astron. Astrophys.* **140**, 243–250 (1984)
- R. Lallement, J.-L. Bertaux, F. Dalaudier, Interplanetary Lyman α spectral profiles and intensities for both repulsive and attractive solar force fields predicted absorption pattern by a hydrogen cell. *Astron. Astrophys.* **150**, 21–32 (1985a)
- R. Lallement, J.-L. Bertaux, V.G. Kurt, Solar wind decrease at high heliographic latitudes detected from Prognoz interplanetary Lyman α mapping. *J. Geophys. Res.* **90**, 1413–1423 (1985b)
- R. Lallement, E. Quémerais, J.-L. Bertaux, S. Ferron, D. Koutroumpa, R. Pellinen, Deflection of the interstellar neutral hydrogen flow across the heliospheric interface. *Science* **307**, 1447–1449 (2005)
- R. Lallement, E. Quémerais, D. Koutroumpa, J.-L. Bertaux, S. Ferron, W. Schmidt, P. Lamy, The interstellar H flow: updated analysis of SOHO/SWAN Data. *AIP Conf. Proc.* **1216**, 555–558 (2010)
- M. Lee, H. Kucharek, E. Möbius et al., An analytical model of interstellar gas in the heliosphere tailored to interstellar boundary explorer observations. *Astrophys. J. Suppl.* **198**, article id 10 (2012)
- P. Lemaire, C. Emerich, W. Curdt et al., Solar H I Lyman alpha full disk profile obtained with the SUMER/SOHO spectrometer. *Astron. Astrophys.* **334**, 1095–1098 (1998)

- B.G. Lindsay, R.F. Stebbings, Charge transfer cross sections for energetic neutral atom data analysis. *J. Geophys. Res.* **110**, A12213 (2005)
- J. Linsky, B. Wood, The alpha Centauri line of sight: D/H ratio, physical properties of local interstellar gas, and measurement of heated hydrogen (the “hydrogen wall”) near the heliopause. *Astrophys. J.* **463**, 254 (1996)
- L.J. Maher, B.A. Tinsley, Atomic hydrogen escape rate due to charge exchange with hot plasmaspheric ions. *J. Geophys. Res.* **82**, 689–695 (1977)
- Y.G. Malama, Monte-Carlo simulation of neutral atoms trajectories in the solar system. *Astrophys. Space Sci.* **176**, 21–46 (1991)
- Y.G. Malama, V.V. Izmodenov, S.V. Chalov, Modeling of the heliospheric interface: multi-component nature of the heliospheric plasma. *Astron. Astrophys.* **445**, 693–701 (2006)
- D.J. McComas, R.W. Ebert, H.A. Elliott et al., Weaker solar wind from the polar coronal holes and the whole Sun. *Geophys. Res. Lett.* **35**, L18103 (2008)
- D.J. McComas, F. Allegrini, P. Bochsler et al., Global observations of the interstellar interaction from the interstellar boundary explorer (IBEX). *Science* **v326**, 959 (2009)
- R.R. Meier, Some optical and kinetic properties of the nearby interstellar gas. *Astron. Astrophys.* **55**, 211–219 (1977)
- D.C. Morton, J.D. Purcell, Observations of the extreme ultraviolet radiation in the night sky using an atomic hydrogen filter. *Planet. Space Sci.* **9**, 455–458 (1962)
- H.-R. Mueller, V. Florinski, J. Heerikhuizen, V.V. Izmodenov, K. Scherer, D. Alexashov, H.-J. Fahr, Comparing various multi-component global heliospheric models. *Astron. Astrophys.* **491**, 43–51 (2008)
- M. Neugebauer, C.W. Snyder, Solar plasma experiment. *Science* **138**, 1095 (1962)
- M. Opher, F.A. Bibi, G. Toth, J.D. Richardson, V.V. Izmodenov, T.I. Gombosi, A strong, highly-tilted interstellar magnetic field near the Solar System. *Nature* **462**, 1036–1038 (2009)
- E.N. Parker, Dynamics of the interplanetary gas and magnetic fields. *Astrophys. J. Lett.* **128**, 664 (1958)
- E.N. Parker, The stellar-wind regions. *Astrophys. J. Lett.* **134**, 20–27 (1961)
- T.N.L. Patterson, F.S. Johnson, W.B. Hanson, The distribution of interplanetary hydrogen. *Planet. Space Sci.* **11**, 767–778 (1963)
- W.R. Pryor, J.M. Ajello, C.A. Barth et al., The Galileo and Pioneer Venus ultraviolet spectrometer experiments: solar Lyman-alpha latitude variation at solar maximum from interplanetary Lyman-alpha observations. *Astrophys. J.* **394**, 363–377 (1992)
- W.R. Pryor, J.L. Scott, I.F. Stewart et al., Interplanetary Lyman α observations from Pioneer Venus over a solar cycle from 1978 to 1992. *J. Geophys. Res.* **103**, 26833–26849 (1998)
- W.R. Pryor, J.M. Ajello, D.J. McComas, M. Witte, W.K. Tobiska, Hydrogen atom lifetimes in the three-dimensional heliosphere over the solar cycle. *J. Geophys. Res.* **108**, 8034 (2003). doi:10.1029/2003JA009878
- E. Quémerais, Angle dependent partial frequency redistribution in the interplanetary medium at Lyman α . *Astron. Astrophys.* **358**, 353–367 (2000)
- E. Quémerais, V.V. Izmodenov, Effects of the heliospheric interface on the interplanetary Lyman α glow seen at 1 AU from the Sun. *Astrophys.* **396**, 269–281 (2002)
- E. Quémerais, R. Lallement, J.-L. Bertaux et al., Interplanetary Lyman α line profiles: variations with solar activity cycle. *Astron. Astrophys.* **445**, 1135–1142 (2006)
- E. Quémerais, V.V. Izmodenov, D. Koutroumpa, Y.G. Malama, Time dependent model of the interplanetary Lyman α glow: applications to the SWAN data. *Astron. Astrophys.* **448**, 351–359 (2008)
- D. Ruciński, M. Bzowski, Modulation of interplanetary hydrogen density distribution during the solar cycle. *Astron. Astrophys.* **296**, 248–263 (1995)
- N.A. Schwadron, M. Bzowski, G.B. Crew et al., Comparison of interstellar boundary explorer observations with 3D global heliospheric models. *Science* **326**, 966 (2009)
- H. Sherer, M. Bzowski, H.-J. Fahr, D. Ruciński, Improved analysis of interplanetary HST Ly- α spectra using time-dependent modelings. *Astron. Astrophys.* **342**, 601 (1999)

- I.S. Shklovsky, On hydrogen emission in the night glow. *Planet. Space Sci.* **1**, 63–65 (1959)
- E.C. Stone, A.C. Cummings, F.B. McDonald et al., *Science* **309**, 2017–2020 (2005)
- B. Strömgren, The physical state of interstellar hydrogen. *Astrophys. J.* **89**, 526–547 (1939)
- T. Summanen, R. Lallement, J.-L. Bertaux, E. Kyrölä, Latitudinal distribution of solar wind as deduced from Lyman α measurements: an improved method. *J. Geophys. Res.* **98**, 13215–13224 (1993)
- T. Summanen, The effect of the time and latitude-dependent solar ionisation rate on the measured Lyman α -intensity. *Astron. Astrophys.* **314**, 663–671 (1996)
- T. Terasawa, Energy spectrum and pitch angle distribution of particles reflected by MHD shock waves fast mode. *Planet. Space Sci.* **27**, 193–201 (1979)
- G.E. Thomas, Properties of nearby interstellar hydrogen deduced from Lyman α sky background measurements. In C.P. Sonett, P.J. Coleman, J.M. Wilcox (eds.), *Solar Wind*, Scientific and Technical Information Office, National Aeronautics and Space Administration., Washington, p. 661 (1972)
- G.E. Thomas, R.F. Krassa, OGO-5 measurements of the Lyman α sky background. *Astron. Astrophys.* **11**, 218 (1971)
- M.K. Wallis, Local interstellar medium. *Nature* **254**, 202–203 (1975)
- B.Y. Welsh, Warm and hot gas in the local ISM. *Space Sci. Rev.* **143**, 241–252 (2009)
- L. Williams, D.T. Hall, H.L. Pauls, G.P. Zank, The heliospheric hydrogen distribution: a multifluid model. *Astrophys. J.* **476**, 366–384 (1997)
- N. Witt, P.W. Blum, J.M. Ajello, Solar wind latitudinal variations deduced from Mariner 10 interplanetary H 1216 Å observations. *Astron. Astrophys.* **73**, 272–281 (1979)
- N. Witt, P.W. Blum, J.M. Ajello, Polar solar wind and interstellar wind properties from interplanetary Lyman-alpha radiation measurements. *Astron. Astrophys.* **95**, 80–85 (1981)
- F.M. Wu, D.L. Judge, Temperature and flow velocity of the interplanetary gases along solar radii. *Astrophys. J.* **231**, 594–605 (1979)

Cross-Calibration of Far UV Spectra of Solar System
Objects and the Heliosphere

Quémerais, E.; Snow, M.; Bonnet, R.-M. (Eds.)

2013, VII, 275 p., Hardcover

ISBN: 978-1-4614-6383-2